eNeuro

Research Article: New Research | Cognition and Behavior

What makes eye contact special? Neural substrates of on-line mutual eye-gaze: a hyperscanning fMRI study

Takahiko Koike[1,2], Motofumi Sumiya[1,2], Eri Nakagawa[1], Shuntaro Okazaki[1] and Norihiro Sadato[1,2,3]

[1]*Division of Cerebral Integration, Department of System Neuroscience, National Institute for Physiological Sciences (NIPS), Aichi, 444-8585, Japan*

[2]*Department of Physiological Sciences, School of Life Sciences, The Graduate University for Advanced Studies (SOKENDAI), Kanagawa, 240-0193, Japan*

[3]*Biomedical Imaging Research Center (BIRC), University of Fukui, Fukui, 910-1193, Japan*

https://doi.org/10.1523/ENEURO.0284-18.2019

Received: 12 July 2018

Revised: 27 January 2019

Accepted: 5 February 2019

Published: 25 February 2019

T.K. and N.S. designed research; T.K., M.S., E.N., and S.O. performed research; T.K. analyzed data; T.K. and N.S. wrote the paper; S.O. contributed unpublished reagents/analytic tools.

Funding: JSPS KAKENHI
15H01846
18H04207
15H05875
16K16894

Funding: MEXT KAKENHI
15K12775

Funding: http://doi.org/10.13039/100009619Japan Agency for Medical Research and Development (AMED)
JP18dm0107152h0003

Funding: http://doi.org/10.13039/501100005806Hayao Nakayama Foundation for Science and Technology and Culture

Conflict of Interest: We have no conflicts of interest to declare.

Correspondence should be addressed to Norihiro Sadato, sadato@nips.ac.jp

Cite as: eNeuro 2019; 10.1523/ENEURO.0284-18.2019

What makes eye contact special? Neural substrates of on-line mutual eye-gaze: a hyperscanning fMRI study

Abbreviated title: Neural substrates of on-line mutual eye-gaze

Takahiko Koike[1,2], Motofumi Sumiya[1,2], Eri Nakagawa[1], Shuntaro Okazaki[1], and Norihiro Sadato[1,2,3]

[1] Division of Cerebral Integration, Department of System Neuroscience, National Institute for Physiological Sciences (NIPS), Aichi, Japan 444-8585

[2] Department of Physiological Sciences, School of Life Sciences, The Graduate University for Advanced Studies (SOKENDAI), Kanagawa, Japan 240-0193

[3] Biomedical Imaging Research Center (BIRC), University of Fukui, Fukui, Japan 910-1193

Author contributions: TK and NS designed research: TK, MS, EN, and SO performed research; TK analyzed data; and TK and NS wrote the paper.

Corresponding author:

Norihiro Sadato, MD, PhD

Division of Cerebral Integration, National Institute for Physiological Sciences, Okazaki, 444-8585, Japan

Email: sadato@nips.ac.jp;

Phone: +81-564-55-7841; Fax: +81-564-55-7843

Number of figures: 6

Number of tables: 4

Abstract: 241 words

Significance statement: 65 words

Introduction: 710 words

Discussion: 2524 words

Acknowledgments

Conflicts of Interest

We have no conflicts of interest to declare.

Funding sources

This study was supported by JSPS KAKENHI #15H01846 to NS, MEXT KAKENHI #15K12775, JSPS KAKENHI #18H04207 and JSPS KAKENHI #15H05875 to TK, and JSPS KAKENHI #16K16894 to EN. This research is partially supported by the Strategic Research Program for Brain Sciences from Japan Agency for Medical Research and Development (AMED) under grant number JP18dm0107152h0003 and by the HAYAO NAKAYAMA Foundation for Science & Technology and Culture.

Abstract

Automatic mimicry is a critical element of social interaction. A salient type of automatic mimicry is eye contact characterized by sharing of affective and mental states among individuals. We conducted a hyperscanning functional magnetic resonance imaging (fMRI) study involving online (LIVE) and delayed off-line (REPLAY) conditions to test our hypothesis that recurrent interaction through eye contact activates the limbic mirror system, including the anterior cingulate cortex (ACC) and anterior insula (AIC), both of which are critical for self-awareness. Sixteen pairs of human adults participated in the experiment. Given that an eye-blink represents an individual's attentional window toward the partner, we analyzed pairwise time-series data for eye-blinks. We used multivariate autoregression analysis to calculate the noise contribution ratio (NCR) as an index of how a participant's directional attention was influenced by that of their partner. NCR was greater in the LIVE than in the REPLAY condition, indicating mutual perceptual–motor interaction during real-time eye contact. Relative to the REPLAY condition, the LIVE condition was associated with greater activation in the left cerebellar hemisphere, vermis, and ACC, accompanied by enhanced functional connectivity between ACC and right AIC. Given the roles of the cerebellum in sensorimotor prediction and ACC in movement initiation, ACC–cerebellar activation may represent their involvement in modulating visual input related to the partner's movement, which may, in turn, involve the limbic mirror system. Our findings indicate that mutual interaction during eye contact is mediated by the cerebellum and limbic mirror system.

Significance Statement (65 words)

Eye contact is a key element that connects humans during social communication. We focused on a previously unaddressed characteristic of eye contact: real-time mutual interaction as a form of automatic mimicry. Our results indicate that real-time interaction during eye contact is mediated

by the cerebellum and limbic mirror system. These findings underscore the importance of the mirror system and cerebellum in real-time unconscious social interaction.

Introduction

Automatic mimicry refers to unconscious or automatic imitation of movement (Prochazkova and Kret, 2017). It is a critical part of human social interaction because it is closely tied to the formation of relationships and feeling of empathy (Chartrand and van Baaren, 2009). Automatic mimicry occurs when two or more individuals engage in the same behavior within a short window of time (e.g., facial expressions, body postures, laughter, yawning) (Prochazkova and Kret, 2017). Automatic mimicry induces synchronous behavior through recurrent interaction (Okazaki et al. 2015), thereby enabling spontaneous synchronization (e.g., clapping) and goal-directed cooperation (Sebanz et al., 2006).

Eye contact is one of the most salient types of automatic mimicry, as two people must be able to synchronize their eye movements to make eye contact (Prochazkova and Kret, 2017). Eye gaze provides a communicative signal that transfers information regarding emotional and mental states (Emery, 2000). Eye contact, or mutual gaze, conveys the message, "I am attending to you," thereby promoting effective communication and enhancing social interaction (Farroni et al., 2002; Schilbach, 2015).

Recent functional MRI studies have revealed that eye contact activates the social brain, including the fusiform gyrus (George et al., 2001; Calder et al., 2002; Pageler et al., 2003), anterior (Calder et al., 2002; Wicker et al., 2003) and posterior superior temporal gyri (Pelphrey et al., 2004; Schilbach et al., 2006; Conty et al., 2007), medial prefrontal cortex (Calder et al., 2002; Kampe et al., 2003; Schilbach et al., 2006; Conty et al., 2007), orbitofrontal cortex (Wicker et al., 2003; Conty et al., 2007), and amygdala (Kawashima et al., 1999; Wicker et al.,

2003; Sato et al., 2004) (see Senju and Johnson, 2009 for review). The abovementioned studies were conducted using single-participant functional magnetic resonance imaging (fMRI) data, contrasting the neural activation elicited by an eye-contact event with that elicited by an eye-aversion event. However, neural substrates underlying recurrent interaction during eye contact that result in the development of shared, pair-specific psychological states (e.g., attention and emotion) remain unknown.

The mirror neuron system plays a role during mutual interaction through joint attention (Saito et al. 2010; Koike et al. 2016). The existence of two main networks with mirror properties has been demonstrated: one residing in the parietal lobe and premotor cortex plus caudal part of the inferior frontal gyrus (parieto-frontal mirror system), and the other formed by the insula and anterior medial frontal cortex (limbic mirror system) (Cattaneo and Rizzolatti, 2009). The parieto-frontal mirror system is involved in recognizing voluntary behavior, while the limbic mirror system is devoted to recognizing affective behavior (Cattanero and Rizzolatti 2009). We hypothesized that mutual interaction involving eye contact activates the limbic mirror system.

This study aimed to elucidate the behavioral and neural representations of mutual interaction during eye contact using hyperscanning fMRI (Koike et al., 2016). The neural activity associated with real-time eye contact was compared with that of non-real-time eye contact using a double-video system (Murray and Trevarthen, 1985). Eye contact is characterized by a two-way, behavioral stimulus-to-brain coupling, such that the behavior of a partner is coupled to the activation in the brain of the other (Hari and Kujala, 2009). Thus, face-to-face interaction through eye contact can be regarded as a mirrored reactive–predictive controller system consisting of two controllers (Wolpert et al., 2003). We used eye-blink as a behavioral index of mutual exchange of communicative cues between two participants during

eye contact. As the blinks of others can be easily recognized due to their relatively long duration (200–400 ms, VanderWerf et al. 2003), eye blinks can provide social communication cues (Nakano and Kitazawa, 2010). Further, blink rates change with internal states such as arousal, emotion, and cognitive load (Ponder and Kennedy, 1927; Hall, 1945; Stern et al., 1984). Finally, the timing of eye-blinks is associated with implicit (Herrmann, 2010) and explicit (Orchard and Stern, 1991) attentional pauses in task content. Nakano and Kitazawa (2010) observed that eye blinks of a listener and speaker were synchronized during face-to-face conversations, and concluded that eye-blinks define the attentional temporal window and that its synchronization reflects smooth communication between interactants through sharing of attention in the temporal domain. In this study, we used hyperscanning fMRI to analyze brain activation related to eye-blinks using different measures: activation, modulation of functional connectivity, and inter-brain synchronization.

Materials and Methods

Participants

Thirty-four volunteers participated in the experiment (20 men, 14 women; mean age ± standard deviation: 21.8 years ± 2.12 years). Participant pairs were determined prior to the experiment, and consisted of participants of the same sex. None of the participants had met each other prior to the experiment. All participants except one were right-handed, as evidenced by the Edinburgh Handedness Inventory (Oldfield, 1971). None of the participants had a history of neurological or psychiatric illness. The protocol was approved by the ethics committee of the Institute. The study was conducted in compliance with the national legislation and the Code of Ethical Principles for Medical Research Involving Human Subjects of the World Medical Association (Declaration of Helsinki). All participants provided written informed consent prior to the experiment.

Design and Procedure

Experimental setup

In order to measure neural activation during the online exchange of eye signals between pairs of participants, we used a hyperscanning paradigm with two MRI scanners (Magnetom Verio 3T, Siemens, Erlangen, Germany) installed side-by-side in parallel, sharing one control room and a triggering system (Morita et al., 2014; Koike et al., 2016). The top component of the standard 32-channel coil was replaced by a small four-channel flex coil (Siemens) attached with a special holding fixture (Takashima Seisakusho, Tokyo, Japan) (Morita et al., 2014; Koike et al., 2016) to fully visualize the eye region. Online grayscale video cameras were used during scanning to identify reciprocal face-to-face interaction (NAC Image Technology, Tokyo, Japan). The cameras captured images of each participant's face, including

158 the eyes and eyebrows. The captured images were in turn projected using a liquid crystal display
159 (LCD) projector (CP-SX12000J, Hitachi, Tokyo, Japan) onto a half-transparent screen that
160 stood behind the scanner bed. The captured images were also entered into the picture delay
161 system (VM-800, Sugioka System, Osaka, Japan), which could output video delayed by an
162 arbitrary amount of time. For analysis, video pictures used in the experiment were transferred to
163 a video recording system (Panasonic, Osaka, Japan). We recorded facial movement in AVI
164 format (640 × 480 pixels, 30 frames/s). While the exact values varied depending on the
165 participant's head size, the screen stood approximately 190 cm from the participants' eyes, and
166 the stimuli were presented at a visual angle of 13.06° × 10.45°. The delay between the capture
167 and projection of the participants' face was controlled using a hardware device (VM-800, Ito Co.,
168 Ltd., Osaka, Japan) connected between the video camera and projector. The delay was set at 20 s
169 for the REPLAY condition and 0 s for the LIVE condition. The intrinsic delay of the online video
170 system in this experimental setup was approximately 100 ms.
171
172 *Experimental conditions*
173 We adopted a conventional blocked design for this study. Each run included three
174 conditions: LIVE, REPLAY, and REST. During the LIVE condition, participants were presented
175 with a live video of their partner's face in real time (Figure 1B), allowing for the online
176 exchange of information between the two participants. We instructed participants to gaze into
177 the right or left eye of their partners and think about their partner: what he/she is thinking about,
178 what is his/her personality, how he/she is feeling. The participants were instructed not to exhibit
179 explicit facial expressions such as laughing or grimacing. We also informed them that we will
180 stop MRI scanning if they were not gazing into the partner's eyes for an extended period of time.
181 The REPLAY condition was identical to the LIVE condition, except that the participant watched

a video picture of their partner's face presented at a delay of 20 s. Therefore, there was no real-time interaction between the participants (Figure 1C). During the REPLAY condition, the participant was informed that all the videos they were watching represented their partner's face in real-time. During the REST condition (baseline), participants were required to gaze at the blank screen (Figure 1A). Although we monitored the participants to ensure that they do not fall asleep, two participants fell asleep during the experiment, and we had to restart the experiment after a short break.

Before starting the run, a live video of the partner was presented on the screen to confirm that an interactive partner was in the other scanner. Following confirmation, the video was turned off. The first run began with the REST condition for 30 s, followed by the LIVE, REPLAY, and REST conditions for 20 s each. After each 20-s presentation of the partner's face, the screen was turned off for 1 s, and the condition was switched (i.e., from LIVE to REPLAY, REPLAY to REST, etc.) (Figure 1D). The 1-s interval was designed to prevent participants from becoming aware of the difference between the LIVE and REPLAY conditions. The order of presenting the conditions was pseudo-randomized. The conditions were switched manually during the fMRI run according to a predefined experimental design. Each run consisted of 8 LIVE and 8 REPLAY conditions. The total length of each run was 8 min 30 s, and the entire scan consisted of 4 runs. Throughout the experiment, none of the participants exhibited any sudden display of emotions such as laughter.

An interview following the experiment revealed that only 1 female pair realized that a delayed facial picture was presented in one of the conditions during the experiment; thus, the requirements of the experiment were not fulfilled in the pair. Data were analyzed from the remaining 32 participants (20 men, 12 women; mean age ± standard deviation: 21.8 years ± 2.03 years).

206

207 *MRI data acquisition*

208 Brain activation data were acquired using interleaved T2*-weighted, gradient echo,
209 echo planar imaging (EPI) sequences. Volumes consisted of 60 axial slices, each 2.0-mm thick
210 with a 0.5-mm gap, covering the entire cerebral cortex and cerebellum. The time interval
211 between two successive acquisitions of the same image (repetition time or TR) was 1000 ms,
212 with a flip angle of 80° and echo time (TE) of 30 ms. The field-of-view (FOV) was 192 mm,
213 and the in-plane matrix size was 64 × 64 pixels. We used the multi-band accelerated sequence
214 developed at the University of Minnesota (Moeller et al., 2010), with the multi-band factor set
215 to 6. Thus, 510 volumes (8 min 30 s) were collected for each run. For anatomical reference,
216 T1-weighted high-resolution images were obtained using a three-dimensional
217 magnetization-prepared rapid-acquisition gradient echo sequence (MPRAGE, TR = 1800 ms,
218 TE = 2.97 ms, FA = 9°, FOV = 256 mm, voxel dimensions = 1 × 1 × 1 mm^3) and a full
219 32-channel phased array coil.

220

221 Data analysis

222 *Behavioral data analysis*

223 Extraction of eye-blink time-series

224 Eye-blink was chosen as a behavioral index of interaction during mutual gaze (Koike
225 et al., 2016). We calculated the "*motion energy*" using the AVI video of the participant's face
226 during the task (Schippers et al., 2010) to evaluate the time-series of eye-blinks. Due to
227 technical difficulties with the video recording system, data from 2 pairs were unavailable. In
228 total, video data of faces from 14 pairs (18 men, 10 women; mean age ± standard deviation:
229 21.8 years ± 2.17 years) were subjected to the analysis described below.

Figure 2 illustrates the procedure used to calculate the motion energy time-series representing eye-blinks. First, the spatial window (400 × 100 pixels) of the AVI video was manually set to cover the eye area of each participant. Second, using the pixel intensity of the defined eye area, we obtained the motion energy index, which can detect the occurrence of motion only from a series of pictures (Schippers et al., 2010). The first-order difference in picture intensity was calculated frame-by-frame in each pixel, and the average of the absolute value of differences in each frame was calculated. This process was used to obtain motion energy values at specific time points. The calculation was repeated to obtain the motion energy time-series reflecting eye-blinks during each run. Third, we divided the time-series in each run into shorter sub-sections corresponding to the LIVE, REPLAY, and REST conditions. Although each condition lasted 20 s (Figure 1D), we analyzed only the final 15 s of each condition to minimize the effect of brightness instability (largely due to the procedure for switching conditions). We obtained 8 time-series for each condition of a single run. As each participant underwent 4 runs, 32 time-series were obtained for each condition per participant. Finally, the effect of the linear trend in the data was removed using the "detrend" function implemented in MATLAB. The whole procedure was performed using a MATLAB script (MATLAB 14; Mathworks, Natick, MA, USA) developed in-house.

Number of eye-blinks

To determine whether the number of eye-blinks itself was influenced by differences in the type of task, we calculated the number of eye-blinks in the LIVE, REPLAY, and REST conditions using the extracted time-series of motion energy. We first adapted the peak-detection function implemented in MATLAB, which automatically detected and marked the time-point at which the eye-blink appeared to occur (see Figure 2). Next, we visually examined whether the detected

time-point was acceptable. Finally, we calculated the average number of eye-blinks in 1 block (15 s) for each participant. All calculations were performed using a MATLAB script (MATLAB 2014) developed in-house.

Causality analysis between eye-blink time-series

Several hyperscanning studies have used synchronization or correlation as an index of interaction (Babiloni and Astolfi, 2012; Koike et al., 2016), neither of which can evaluate the directional effect. In this study, we used an Akaike causality model (Akaike, 1968; Ozaki, 2012), which can delineate the causal direction and quantify its effect. The Akaike causality model utilizes a multivariate autoregressive (MVAR) model under the steady state assumption and can quantify the proportion of the power-spectral density of an observed variable from the independent noise of another variable. The quantified causality, that is the noise contribution ratio (NCR) index, is regarded as a measure of how one variable is influenced by another. In this study, we assumed that the eye-blink time-series satisfies a steady state assumption at least in one block. The NCR values were calculated as follows.

First, an MVAR model was applied to a pair of time-series data, x(t) and y(t), using the linear sum of the history of the two time-series, as follows:

$$x(t)=\sum_{i=1}^{N}a_i x(t-i)+\sum_{i=1}^{N}b_i y(t-i)+u_x(t) \qquad \text{(Eq. 1)}$$

$$y(t)=\sum_{i=1}^{N}c_i x(t-i)+\sum_{i=1}^{N}d_i y(t-i)+u_y(t), \qquad \text{(Eq. 2)}$$

where the time-series $x(t)$ and $y(t)$ correspond to the time-series of the participant's eye-blinks and that of the partner, respectively. In these equations, a_i, b_i, c_i, and d_i

indicate AR coefficients, while u_x and u_y indicate the residual noise in the eye blinks of the participant and partner, respectively. The AR order *N* defines the duration of the history. For each pair of time-series data, the AR order N was estimated to minimize the Akaike information criterion in the range from 1 to 10. Next, we estimated the power spectrum of the two time-series based on the sum of the contributions of the *x*-specific noise (i.e., $|\alpha(f)|^2 \sigma_{ux}{}^2$) and *y*-specific noise (i.e., $|\beta(f)|^2 \sigma_{uy}{}^2$). Here, $\alpha(f)$ and $I2(f)$ are frequency response functions, derived from Fourier transformation via an impulse response function, using a set of AR coefficients, while σ_{ux} and σ_{ux} indicate the variance of residual noise u_x and u_y, respectively. The $NCR_{y\to x}(f)$, an index reflecting how the participant's eye blinks $x(t)$ are influenced by the partner's eye-blinks $y(t)$, was calculated from the ratio of part of the spectral density of $x(t)$ contributed by $\sigma_{uy}{}^2$ to the total spectral density of $x(t)$ at frequency *f*. Therefore, $NCR_{y\to x}(f)$ can be expressed as follows:

$$NCR_{y\to x}(f) = \frac{|\beta(f)|^2 \sigma_{uy}{}^2}{|\alpha(f)|^2 \sigma_{ux}{}^2 + |\beta(f)|^2 \sigma_{uy}{}^2}. \qquad \text{(Eq. 3)}$$

To assess how $x(t)$ is influenced by $y(t)$ across the whole frequency range, we mathematically integrated *NCR* values via trapezoidal numerical integration as follows:

$$\Sigma NCR_{y\to x} = \int_0^{f_s/2} NCR_{y\to x}(f)df, \qquad \text{(Eq. 4)}$$

where f_s is the sampling frequency of the time-series $x(t)$ and $y(t)$. In this study, f_s was 30 Hz, based on the frame rate of the video data. We collected 32 time-series for each condition. Therefore, our calculations yielded 32 *ΣNCR* values for each condition per participant. These 32

294 *ΣNCR* values were averaged to calculate one summarized *ΣNCR* value for each participant in
295 each condition. Using the summarized *ΣNCR*, we applied statistical analyses to determine
296 whether the influence of the partner differed between conditions. The entire procedure was
297 performed using a MATLAB script (MATLAB 2014) written in-house.

298 In this study, we calculated four *ΣNCR* values to assess how a participant's eye-blink
299 was influenced by that of the partner. Firstly, in the REST condition, participants could see
300 nothing on the screen. Therefore, the ΣNCR value in the REST condition, i.e. $\Sigma\mathrm{NCR}_{F\to F}^{REST}$, was
301 regarded as a baseline of causal relationship. In the LIVE condition, the face of one participant
302 was immediately projected on the screen, and the partner was able to see the face in real time. In
303 this condition, we calculated ΣNCR between two participants' time-series, i.e. $\Sigma\mathrm{NCR}_{F\to F}^{LIVE}$. The
304 ΣNCR value represents how participants influence their partners when they mutually interact
305 with each other in real-time. Next, in the REPLAY condition, two types of causality were
306 calculated- first, the ΣNCR value between actual eye-blinks, like in the LIVE condition, i.e.
307 $\Sigma\mathrm{NCR}_{F\to F}^{REPLAY}$; and second, the ΣNCR value in the REPLAY condition representing how the
308 eye-blinks projected on the screen has an influence on the actual eye-blink time series,
309 $\Sigma\mathrm{NCR}_{S\to F}^{REPLAY}$. While it is possible that a participant's face receives influence from the delayed
310 picture on the screen (Nakano and Kitazawa, 2010), influence from an actual eye-blink to the
311 screen (reverse-influence) is theoretically absent. We also calculated the ΣNCR value, i.e.
312 $\Sigma\mathrm{NCR}_{F\to F}^{REST}$. It represents how participants are influenced by video picture, while there could be
313 only unidirectional influence from the screen to actual eye-blinks.
314
315 Estimation of statistical inferences and data visualization
316 All statistical inference estimation for the behavioral data analysis was performed
317 using R (RRID: SCR_001905). We analyzed three types of behavioral measures. (1) The

number of eye-blinks is highly influenced by the degree of attention (Ponder and Kennedy, 1927; Hall 1945; Stern et al. 1984; Herrmann, 2010; Orchard and Stern, 1991) and could reflect the differences across conditions. We tested the number of eye-blinks in three conditions using repeated-measures analysis of variance (ANOVA). (2) ΣNCR values: We have four ΣNCR values for each participant- $\Sigma NCR_{F\rightarrow F}^{REST}$ in the REST condition, $\Sigma NCR_{F\rightarrow F}^{REPLAY}$ and $\Sigma NCR_{S\rightarrow F}^{REPLAY}$ in the REPLAY condition, and $\Sigma NCR_{F\rightarrow F}^{LIVE}$ in the LIVE condition. The differences between them were assessed using repeated-measures ANOVA. (3) Enhanced ΣNCR values: In the REST condition, participants know there is no interaction with a partner as nothing is projected on the screen. Therefore, theoretically speaking, the REST condition could be regarded as a baseline condition. We calculated the increase in ΣNCR values (enhancement) by subtracting the $\Sigma NCR_{F\rightarrow F}^{REST}$ value from each of the ΣNCR values. Thus, we have three enhanced ΣNCR values for each participant: $\Sigma NCR_{F\rightarrow F}^{LIVE} - \Sigma NCR_{F\rightarrow F}^{REST}$,$\Sigma NCR_{F\rightarrow F}^{REPLAY}$-$\Sigma NCR_{F\rightarrow F}^{REST}$, and $\Sigma NCR_{S\rightarrow F}^{REPLAY} - \Sigma NCR_{F\rightarrow F}^{REST}$. Repeated-measures ANOVA was used to test the differences between these values. In all ANOVA procedures, the effect size was measured using the generalized eta-squared value (Olejnik and Algina, 2003). In the post-hoc pair-wise analysis, estimated p-values were adjusted using Bonferroni correction. The confidence levels for post-hoc pair-wise analyses were calculated via Franz-Loftus's pair-wise confidence intervals (Franz and Loftus, 2012). The details of the statistical methods used in this behavioral data analysis are listed in Table 1. All the graphs were prepared using the RainCloudPlots R-script (Allen et al., 2018) (https://github.com/RainCloudPlots/RainCloudPlots), which could provide a combination of box, violin, and dataset plots. In the dataset plot, each dot represents a data point, respectively. Outliers were defined by two standard deviations and are represented in Figure 2 by red diamonds. In the boxplot, the line dividing the box represents the median of the data, while the ends of the box represent the upper and lower quartiles. The extreme lines show the highest and

lowest values excluding outliers defined by 2.0 standard deviations.

Neuroimaging analysis

Image preprocessing

The first 10 volumes (10 s) of each fMRI run were discarded to allow for stabilization of the magnetization, and the remaining 500 volumes per run (total of 2,000 volumes per participant) were used for the analysis. The data were analyzed using statistical parametric mapping (SPM12, Wellcome Trust Center for Neuroimaging, London, UK) (RRID:SCR_007037) implemented in MATLAB 2014 (RRID: SCR_001622). All volumes were realigned for motion correction. The whole-head T1-weighted high-resolution MPRAGE volume was co-registered with the mean EPI volume. The T1-weighted image was normalized to the Montreal Neurological Institute template brain using a nonlinear basis function in SPM12. The same normalization parameters were applied to all EPI volumes. All normalized EPI images were spatially smoothed in three dimensions using a Gaussian kernel (full-width at half-maximum = 8 mm).

Estimation of task-related activation using univariate generalized linear modeling (GLM)

Due to technical difficulties, we could not acquire fMRI data from 1 pair. Therefore, we analyzed whole fMRI data acquired from 30 participants (18 men, 12 women; mean age ± standard deviation: 21.7 years ± 2.10 years). Statistical analysis was conducted at two levels. First, individual task-related activation was evaluated. Second, summary data for each participant were incorporated into a second-level analysis using a random effects model (Friston et al., 1999) to make inferences at a population-level.

In the individual-level analysis, the blood oxygenation level-dependent (BOLD)

time-series representing the brain activation of each participant was first modeled using a boxcar function convolved with a hemodynamic-response function and filtered using a high-pass filter (128 s), while controlling for the effect of runs. Serial autocorrelation assuming a first-order autoregressive model was estimated from the pooled active voxels using the restricted maximum likelihood procedure and used to whiten the data (Friston et al., 2002). No global scaling was applied. The model parameters were estimated using the least-squares algorithm on the high-pass-filtered and whitened data and design matrix. Estimates for each of the model parameters were compared with the linear contrasts to test hypotheses regarding region-specific condition effects. Next, the weighted contrasts of the parameter estimate (i.e., LIVE > REST and REPLAY > REST) in the individual analyses were incorporated into the group analysis. Contrast images obtained via individual analyses represented the normalized task-related increment of the MR signal relative to the control condition (i.e., the REST condition) for each participant.

In the group-level analysis, we investigated differences in brain activation between the LIVE and REPLAY conditions using these contrast images and the random-effect model implemented in SPM12. We analyzed this data using the paired t-test. The resulting set of voxel values for each contrast constituted a statistical parametric map of the t-statistic (SPM {t}). **T**he threshold for significance of the SPM {t} was set at $p < 0.05$ with family-wise error (FWE) correction at the cluster level for the entire brain (Friston et al., 1996). To control family-wise error rates using random field theory (Eklund et al., 2016), the height threshold was set at uncorrected $p < 0.001$, which is conservative enough to depict cluster-level inference with the parametric procedure (Flandin and Friston, 2017). To validate the statistical inference with parametric method, we also tested the statistical significance of activation using a nonparametric permutation test implemented in the SnPM13 toolbox (RRID: SCR_002092; (Nichols and

Holmes, 2002)). We used the non-parametric paired t-test with no variance smoothing; the number of permutations was set at 10000. The SnPM toolbox did not yield statistical significance at all the voxels reported in SPM, thus the p-values for some voxels have not been listed in the tables.

Generalized psycho-physiological interaction analysis

Next, we performed generalized psycho-physiological interaction (gPPI) analysis (Friston et al., 1997; McLaren et al., 2012) using the CONN toolbox (Whitfield-Gabrieli and Nieto-Castanon, 2012) (RRID: SCR_009550) in order to reveal how effective connectivity from the LIVE- or REPLAY-specific regions (towards other brain regions) was altered between the LIVE and REPLAY conditions. For this purpose, we selected three clusters based on the LIVE > REPLAY contrast defined by the results of univariate GLM analysis (Figure 3, Table 2) as seed regions for the gPPI analysis. We used conventional seed-to-voxel gPPI analysis in which the whole brain is the search area. The components associated with a linear trend, cerebrospinal fluid (CSF), white-matter (WM), and experimental tasks (i.e., LIVE and REPLAY effects) were removed from the BOLD time-series as confounding signals. Using the residual time-series, gPPI analysis was performed to evaluate whether the effective connectivity from the seed region was modulated by the task condition (i.e., the LIVE or REPLAY condition) at the individual level. This individual-level analysis produced contrast images representing the modulation of effective connectivity from the seed region. Up to this point, all procedures were conducted using the CONN toolbox. Finally, we used these contrast images and the random-effect model implemented in SPM12 to test whether any regions exhibited significant differences in effective connectivity between the LIVE and REPLAY conditions. Analyses were assessed at $p < 0.05$ with FWE correction at the cluster level. The height threshold to form each cluster was set at an

414 uncorrected p value of 0.001. This relatively high cluster-forming threshold is enough to prevent
415 the failure of multiple-comparison problem in cluster-level statistical inference (Eklund et al.,
416 2016; Flandin and Friston, 2017). We also listed statistical values estimated by the SnPM
417 toolbox with a nonparametric permutation test.
418
419 Inter-brain synchronization analysis
420 We tested for differences in the inter-brain synchronization of the LIVE and REPLAY
421 conditions using conventional voxel-to-voxel method employed by previous hyperscanning
422 fMRI studies that can identify inter-brain synchronization of activation without any prior
423 assumptions (Saito et al., 2010; Tanabe et al., 2012). We focused on the spontaneous fluctuation
424 of BOLD signal that is unrelated to the task-related activation or deactivation (Fair et al., 2007).
425 First, the task-related activation/deactivation was removed from the BOLD time-series using the
426 GLM model implemented in the SPM12. This yielded 3D-Nifti files representing residual
427 time-series that are independent of task-related activation/deactivation compared to baseline, i.e.,
428 the REST condition. Second, we divided the original time-series into three sub-time-series
429 based on the experimental design: LIVE, REPLAY, and REST conditions. Third, we
430 concatenated sub-time-series into one long time-series. The length of the LIVE- and
431 REPLAY-related residual time-series was 640 volumes. Next, we calculated the inter-brain
432 synchronization between the voxels representing the same MNI coordinates (x, y, z) in the two
433 participants using the Pearson's correlation coefficient. This computation was performed using a
434 MATLAB script developed in-house. The correlation coefficient r was transformed to the
435 standardized z-score using Fisher's r-to-z transformation. Finally, we obtained two 3D-Nifti
436 images representing inter-brain synchronization in the LIVE and REPLAY conditions per pair.
437 We conducted the random-effect model analysis in SPM12 at the group level. The

normalized inter-brain synchronization images were used in the group level analysis. Here, the paired t-test was used to test the differences in inter-brain synchronization between the LIVE and REPLAY conditions. The resulting set of voxel values for each contrast constituted a statistical parametric map of the t statistic (SPM {t}). The threshold for significance of the SPM {t} was set at $p < 0.05$ with family-wise error (FWE) correction at the cluster level for the entire brain (Friston et al., 1996); the height threshold was set at an uncorrected p value of 0.001. This cluster threshold is conservative enough to prevent failure in cluster-level inference (Eklund et al., 2016; Flandin and Friston, 2017). The statistical inference was also estimated by a non-parametric permutation test using the SnPM toolbox, like the GLM and gPPI analyses. Anatomical labeling was based on Automated Anatomical Labeling (Tzourio-Mazoyer et al., 2002) and the Anatomy toolbox v1.8 (Eickhoff et al., 2005). Final images have been displayed on a standard template brain image (http://www.bic.mni.mcgill.ca/ServicesAtlases/Colin27) using MRIcron (https://www.nitrc.org/projects/mricron; Rorden & Brett, 2000).

Results

Behavioral index

Figure 3A shows the average number of eye-blinks per block. Repeated-measures ANOVA revealed a significant effect of condition (Table 1, a) ($F(2,54) = 13.1814$, $p < 0.0001$, $\eta_g^2 = 0.0354$). A post-hoc comparison with Bonferroni correction revealed that there were no significant differences in the number of eye-blinks between the LIVE and REPLAY conditions (Table 1, d) ($t(27) = 2.3522$, $p = 0.0786$, Bonferroni correction), while the number of eye-blinks was greater in the REST condition than in the LIVE (Table 1, b) ($t(27) = 3.9464$, $p = 0.0015$, Bonferroni correction) and REPLAY (Table 1, c) ($t(27) = 3.8499$, $p = 0.0021$, Bonferroni correction) conditions.

Next, we compared the *ΣNCR* values using repeated-measures ANOVA (Figure 3B) and found a significant effect of condition was significant ($F(3, 81) = 3.9830$, $p = 0.0295$, $\eta_g^2 = 0.03236$, Table 1, e). A post-hoc comparison with Bonferroni correction revealed that there were significant differences between the $\Sigma NCR_{F\to F}^{LIVE}$ and $\Sigma NCR_{F\to F}^{REPLAY}$ ($T(27) = 3.406$, $p = 0.0126$, Table 1f), $\Sigma NCR_{F\to F}^{LIVE}$ and $\Sigma NCR_{S\to F}^{REPLAY}$ ($T(27) = 3.2934$, $p = 0.0168$, Table 1h). Differences in the other pairs did not meet the threshold for statistical significance (Table 1g, i, j, k). To confirm that the outliers did not skew the parametric statistics, we re-computed the statistical values after removing outliers defined by two standard deviations rather than 1.5. Four subjects to whom the outlier data could be attributed in at least one of the four conditions were excluded from the analysis; the repeated-measures ANOVA therefore included a sample of 24. Even after removing the outliers, the repeated-measures ANOVA could replicate the significant effect of condition ($F(3, 69) = 4.3334$, $p = 0.0074$, $\eta_g^2 = 0.0785$, Table 1l), as well as the significant differences between the $\Sigma NCR_{F\to F}^{LIVE}$ and $\Sigma NCR_{F\to F}^{REPLAY}$ ($T(23) = 3.0965$, $p = 0.0306$, Table 1m), and between $\Sigma NCR_{F\to F}^{LIVE}$ and $\Sigma NCR_{S\to F}^{REPLAY}$ ($T(23) = 3.0779$, $p = 0.0318$, Table 1o). Differences in the other pairs did not meet the threshold for statistical significance (Table 1n, p, q, r).

We also tested differences across enhanced *ΣNCR* values using repeated-measures ANOVA (Figure 3C) and found that the effect of condition was significant ($F(2, 54 = 10.3784$, $p = 0.0002$, $\eta_g^2 = 0.03236$, Table 1s). A post-hoc comparison with Bonferroni correction revealed that there were significant differences between $\Sigma NCR_{F\to F}^{LIVE} - \Sigma NCR_{F\to F}^{REST}$ and $\Sigma NCR_{F\to F}^{REPLAY}$-$\Sigma NCR_{F\to F}^{REST}$ ($T(27) = 3.4061$, $p = 0.0063$, Table 1t), as well as between $\Sigma NCR_{F\to F}^{LIVE} - \Sigma NCR_{F\to F}^{REST}$ and $\Sigma NCR_{S\to F}^{REPLAY} - \Sigma NCR_{F\to F}^{REST}$ ($T(27) = 3.2934$, $p = 0.0084$, Table 1u). Differences in the other pair did not meet the threshold for statistical significance (Table 1v). We recalculated statistical inferences as raw NCR values without outliers to ensure that the

outliers had no effect on the inferences. The stricter criteria for outliers remained two standard deviations, resulting in the removal seven subjects from the analysis. Even after outliers were excluded from the analysis, we obtained qualitatively identical results: significant effect of condition ($F(2, 40) = 7.9233$, $p = 0.0013$, $\eta_g^2 = 0.1330$, Table 1w), and significant differences between $\Sigma NCR_{F\rightarrow F}^{LIVE} - \Sigma NCR_{F\rightarrow F}^{REST}$ and $\Sigma NCR_{F\rightarrow F}^{REPLAY} - \Sigma NCR_{F\rightarrow F}^{REST}$ ($T(20) = 2.8343$, $p = 0.0306$, Table 1x, and between $\Sigma NCR_{F\rightarrow F}^{LIVE} - \Sigma NCR_{F\rightarrow F}^{REST}$ and $\Sigma NCR_{S\rightarrow F}^{REPLAY} - \Sigma NCR_{F\rightarrow F}^{REST}$ ($T(20)=2.9034$, $p=0.0265$, Table 1y). Difference in other pair did not meet the threshold for statistical significance (Table 1z).

To test whether or not these enhancements of entrainment of eye-blinking is influenced by the number of blocks, we calculated the Akaike causality index for separate blocks of the experiment and applied the repeated-measures ANOVA (4 blocks × 4 conditions) to the *ΣNCR* data. We found a significant effect of conditions ($F(3,81)=3.9830$, $p=0.0106$, $\eta_g^2=0.0132$, Table 1aa). However, the effects of sessions ($F(3,81)=1.0351$, $p=0.3816$, $\eta_g^2=0.0139$, Table 1bb) and interaction (session × conditions) ($F(9,243)=1.8235$, $p=0.0647$, $\eta_g^2=0.0128$, Table 1cc) were nonsignificant. Therefore, in the following analysis of neuroimaging data, we combined data from the four blocks.

Brain activation in the LIVE and REPLAY conditions

We used GLM analysis (Table 1dd, ee) to elucidate brain activation in the LIVE and REPLAY conditions. For the LIVE vs. REPLAY contrast, we observed greater activation in the left cerebellar hemisphere (lobule VI, VII, and VIIIa), bilateral paravermis area (lobule XI) (Figure 4A), and the pre-supplementary motor area (pre-SMA) extending to the dorsal tier of the anterior cingulate cortex (ACC) (Figure 4B). No significant differences in activation were observed in the REPLAY vs. LIVE contrast. Detailed information regarding each cluster is

outlined in Table 2.

Results of the gPPI analysis

The gPPI analysis (Table 1ff, gg) revealed that the effective connectivity from the ACC region toward the dorsal anterior insular cortex (dAIC) (Chang et al., 2013) was greater during the LIVE condition than during the REPLAY condition (Figure 4, Table 3). No regions exhibited greater effective connectivity involving the pre-SMA–ACC regions in the REPLAY condition than in the LIVE condition. There was no modulation of effective connectivity involving cerebellar seed regions.

Inter-brain synchronization

Figure 6 illustrates inter-brain synchronization that is specific to the LIVE condition (Table 1hh, ii). It was found on the bilateral middle occipital gyrus (MOG). Detailed information about these clusters is described in Table 4. No regions showed significant inter-brain synchronization in the REPLAY condition compared to the LIVE condition.

Discussion

This study aimed to elucidate the behavioral and neural representations of mutual interaction during eye contact by comparing the neural activity associated with real-time eye contact with that associated with non-real-time eye contact. Our findings suggest that mutual interaction/shared attention during eye contact is mediated by the cerebellum and the limbic mirror system.

Behavioral index

In this study, causal analysis using a multivariate autoregressive (MVAR) model (Akaike, 1968; Ozaki, 2012) was performed to assess how an individual's temporal attentional window is influenced by that of the partner (Schippers et al., 2009; Okazaki et al., 2015; Leong et al., 2017). Our results show that participants were more sensitive to the eye-blinks of a partner in the LIVE condition than in the REPLAY condition as none of the participants perceived the difference between the LIVE and REPLAY conditions. Thus, the experimental setup for our LIVE condition enabled a reciprocal feedback system through the visual modality. Our findings suggest that perceptual–motor interaction occurs during eye contact without conscious awareness. Previous researchers have argued that an essential component of real-time social interactions involves reciprocal coupling via perceptual–motor linkages between interacting individuals (Nicolis and Prigogine, 1977; Haken, 1983; Bernieri and Rosenthal, 1991; Strogatz, 2003; Oullier et al., 2008). Our results extend this notion to the attention mediated by the minimal motion of blinking, which represents the temporal window of attention towards one's partner. Interestingly, the influence from a partner was significantly greater when the information flow between two individuals was reciprocal ($\Sigma NCR_{F\rightarrow F}^{LIVE}$) than when it was unidirectional ($\Sigma NCR_{S\rightarrow F}^{REPLAY}$). As the mutual interaction in real time evinced a significant effect on the partner's eye blink, this finding indicated that the mutual online interaction is critical to the influence of the other's eye blink. Feedback through the on-line mutual interaction may induce a non-linear response, causing the subtle effect to be amplified (Okazaki et al. 2015).

This experiment can be regarded as a simplified version of the social contingency detection task originally reported by Murray and Trevarthen (1985). Social contingency is defined as the cause–effect relationship between one's behavior and consequent social events (Gergely, 2001; Nadel, 2002) and is highly associated with a sense of self or one's own body in

557 infancy, developing a sense of reciprocity, and participation with others (Rochat, 2001), all of
558 which are critical for typical development (Mundy and Sigman, 1989; Gergely, 2001; Goldstein
559 et al., 2003; Kuhl et al., 2003; Watanabe, 2013). Several previous studies have investigated
560 differences in mother–infant interactions between real-time bidirectional interaction and off-line
561 unidirectional interaction (Murray and Trevarthen, 1985; Nadel et al., 2001; Stormark and
562 Braarud, 2004; Soussignan et al., 2006). Even in adults, turn-taking behavior accompanying
563 social contingency is likely to serve as experience-sharing, which represents the basis of all
564 social behaviors (Rochat, 2009; Stevanovic and Peräkylä, 2015). Our results indicate that even a
565 minimal task condition, such as mutual gaze, constitutes a reciprocal feedback system that can
566 provide a basis for the detection of social contingency, promoting sharing of attention between
567 partners (Farroni et al., 2002; Schilbach, 2015).
568
569 Neural substrates of eye-contact in real-time
570 Using a conventional GLM approach, we observed LIVE-specific activation in the
571 cerebellum and ACC. The cerebellum plays a key role in error detection and processing of
572 temporal contingency (Blakemore et al., 2003; Trillenberg et al., 2004; Matsuzawa et al., 2005),
573 the latter of which is critical for real-time social communication (Gergely and Watson, 1999).
574 The cerebellum is also critically involved in sensorimotor prediction (Blakemore and Sirigu,
575 2003), especially in building predictions about the actual sensory consequences of an executed
576 motor command. One previous fMRI study reported that the prediction error caused by sensory
577 feedback is essential for acquiring internal forward models of movement control (Imamizu et al.,
578 2000). This prediction (forward model) is mainly used in the early stages of movement
579 execution to maintain accurate performance in the presence of sensory feedback delays
580 (Wolpert and Kawato, 1998), as well as in social interaction (Wolpert et al., 2003). Considering

that real-time social interaction can be regarded as a cross-individual sensorimotor loop (Wolpert et al., 2003; Froese and Fuchs, 2012), the cerebellum may receive visual afferents of the partner's blink as sensory feedback for the prediction of one's blink movement, in order to evaluate temporal contingency between the partners' blinks.

In humans, the ACC is located in the medial wall of the cerebral hemisphere, adjacent to the pre-SMA (Habas, 2010). The ventral (limbic) tier occupies the surface of the cingulate gyrus, corresponding to Brodmann's areas 24a and 24b, and subcallosal area 25. The dorsal (paralimbic) tier is buried in the cingulate sulcus, corresponding to Brodmann's areas 24c and 32 (see Paus, 2001 for a review). The dorsal tier is involved in volitional motor control (Deiber et al., 1996; Picard and Strick, 1996; Brázdil et al., 2006).

The ACC and cerebellum constitute a tightly connected cortico-cerebellar network. Recent functional connectivity analysis studies have demonstrated that distinct cerebellar seed regions in the anterior portion of the crus I exhibit functional connectivity with the dorsolateral prefrontal cortex, the rostral portion of the inferior parietal lobule, and a frontal midline region bordering the pre-SMA and ACC in healthy adults (Buckner et al., 2011; Riedel et al., 2015). Conversely, the ACC exhibits a negative correlation with the cerebellum (Margulies et al., 2007), possibly reflecting its hypothesized role in the inhibition of pre-potent stereotyped responses (Paus et al., 1993; Paus, 2001). In terms of anatomical connectivity, Zalesky et al. (2014) used diffusion MRI to demonstrate disruption of white matter connectivity between the cerebellum and the cingulate cortex in individuals with Friedreich ataxia, an autosomal recessive disease involving degeneration of the spinal cord and cerebellum, thereby supporting the notion of reverse cerebellar diaschisis (Schmahmann and Sherman, 1998).

The cortico–cerebellar–thalamo–cortical circuit involving the cerebellum and ACC plays a role in attention. The cerebellum is involved in attention, including

anticipation/prediction of the internal conditions for a particular operation, as well as the setting of specific conditions in preparation for that operation (Allen et al., 1997; Schweizer et al., 2007). Honey et al. (2005) reported that patients with schizophrenia exhibited an attenuated response of the ACC and cerebellum to degradation of the target during a continuous performance task, paralleling their limited visual attentional resources. They also observed disruption in the pattern of task-related connectivity of the ACC to the prefrontal regions. Honey et al. (2005) concluded that attentional impairments associated with schizophrenia could be attributed to the cortico–cerebellar–thalamo–cortical circuit, which includes the ACC and cerebellum. Considering the role of the ACC and cerebellum in sensorimotor and attentional control, the ACC–cerebellar network may constitute a reactive–predictive controller system (Noy et al., 2011) by which one's own attention-contingent motor output (that is, eye-blink) is modulated by the visual input of the partner's movement. Under the mirror-configuration during the LIVE condition, the reactive-predictive controllers in two individuals work to coordinate their own behavior with the partner's. Thus, it closes the sensorimotor circuits across the individuals.

Enhanced connectivity between the ACC and AIC

We observed enhanced effective connectivity from the ACC to the right dorsal region of the AIC (dAIC) in the LIVE condition than in the REPLAY condition. In the present study, no emotional processes were included in the task, suggesting that the enhancements in connectivity were related to recurrent interaction via eye contact. The ACC has a strong connection to the AIC (Margulies et al., 2007; Taylor et al., 2009; Ghaziri et al., 2015), most prominently in the dAIC (Chang et al., 2013), a central hub in which several different cognitive networks converge (Dosenbach et al., 2006; Chang et al., 2013). The ACC-AIC network

represents the portion of the limbic mirror system related to the recognition of affective behavior (Cattaneo & Rizzolatti, 2009; Fabbri-Destro et al., 2008; Singer et al. 2004).

Medford and Critchley (2010) proposed that the AIC and ACC represent the basis of self-awareness by constituting the input (AIC) and output (ACC) components of a system. In such a system, the integrated awareness of cognitive, affective, and physical states first generated by the integrative functions of the AIC are then re-represented in the ACC as a basis for the selection of and preparation for responses to inner or outer events. Craig (2009) regarded the AIC as the probable site for awareness, based on its afferent representation of "feelings" from the body, and the ACC as the probable site for the initiation of behaviors. Meltzoff (2005) proposed a "like-me" framework for the understanding of others. He suggested that imitation enables understanding of another mind based on an understanding of actions and their underlying mental states. Singer et al. (2004) observed that pain empathy relies on neural structures that are also involved in the direct experience of that emotion (i.e., the limbic mirror system (ACC, AIC)). This finding is consistent with the Simulation Theory, which proposes that "we understand other people's minds by using our mental states to simulate how we might feel or what we might think in a given situation" (Lamm and Singer 2010). Lamm and Singer (2010) concluded that perceiving the states of another activates neural representations encoding each state when it is experienced personally. In the eye-contact state, participants are aware that they are attending to their partner during eye contact. Therefore, given that the ACC–AIC network represents self-awareness, its activation during real-time eye contact may represent a shared mental state (i.e., awareness involving the participant and partner) such as shared attention. This interpretation is consistent with a study by Hietanen et al. (2008), which demonstrated that autonomic arousal is enhanced by eye contact with a live human, but not with static images of faces. The authors argued that this might be due to the enhancement of self-awareness by the

presence of another person. The results of our study suggest that the self-awareness is enhanced by the social contingency generated with live humans through the interaction of each other's attentional windows via eye-blinks and that the regulation of self-awareness by interaction might be caused by the cerebellar–cerebral networks that tap into the limbic mirror system.

Inter-brain synchronization

By comparing the degree of inter-brain synchronization between the LIVE and REPLAY conditions, we found an enhancement in the MOG region related to the LIVE condition. This region is in the lateral occipitotemproral cortex (LOTC) and is almost identical to the region that shows inter-brain synchronization specific to eye-contact state (Koike et al., 2016). Previous studies suggest that the LOTC receives both sensory inputs of a partner's behavior (Lingnau and Downing 2015) and efference copies of one's own behavior (Astafiev et al., 2004; Orlov et al., 2010). Therefore, the roles of the LOTC in supporting action perception and overt action performance are closely related. The LOTC may play a role in the human action observation network (Caspers et al. 2010) that is typically attributed to the frontoparietal mirror system (Oosterhof et al. 2013). Thus, the MOG region may conceivably receive information about self and other's eye-blinks.

Based on the electroencephalography (EEG) hyperscanning experiment of the mutual gaze between mothers and infants, Leong et al. (2017) found interpersonal neural synchronization. They argued that the phase of cortical oscillations reflects the excitability of underlying neuronal populations to incoming sensory stimulation (Schroeder and Lakatos, 2009), a possible mechanism for temporal sampling of the environment (Giraud and Poeppel, 2012). Interpersonal neural synchronization could increase within a dyad during the course of social interaction because each partner is continuously producing salient social signals (such as gaze)

677 that act as synchronization triggers to reset the phase of his or her partner's ongoing oscillations
678 (Leong et al. 2017). The present study showed neural synchronization in the LOTC, which
679 receives both visual input of others' actions and efference copies of one's own actions. The
680 salient social signals sent to the partner through gaze or blink (defining the temporal attentional
681 window), the motor command corresponding to which is likely delivered to the LOTC as an
682 efference copy. The eye-blink may, thus, act as a synchronization trigger. Therefore, the
683 cross-individual neural synchronization of the MOG represents the alignment of the temporal
684 pattern of attention, which may optimize communicative efficiency (Leong et al. 2017).
685
686 Limitations and future directions
687 The present study is subject to several limitations. First, concerning the
688 hyperscanning-fMRI experimental design, the very long mutual gaze condition was not
689 ecological and may be quite different from conceptions of 'mutual gaze' or 'eye-contact'
690 informed by daily life. This is due to our use of a blocked-design, the most effective way to
691 detect brain activation. Also, the product of our experimental design, estimations of the
692 temporal dynamics of eye-blink entrainment, brain activation, and inter-brain synchronization
693 could not be performed. While we could not find a significant effect of session on the eye-blink
694 entrainment in real-time eye-contact, it is possible that the eye-blinking entrainments only occur
695 in the very first phase of mutual gaze condition in one block. By refining the experimental and
696 analytical design, we may further gain insight into the dynamics of inter-individual interaction
697 through eye-contact and inter-brain synchronization. To explore the temporal dynamics of
698 inter-brain synchronization, we are currently conducting a hyperscanning simultaneous
699 EEG-fMRI recording that could integrate the merits of the two neuroimaging methods (Koike et
700 al., 2015). As the present study demonstrated the efficacy of using Akaike causality analysis to

evaluate dynamic mutual interaction, future studies applying this method to EEG data in ecological settings of normal and diseased populations are warranted.

The present study is also limited by its capacity only to find inter-brain synchronization between homologous regions, but not between non-homologous regions – i.e., fronto-parietal synchronization (Dumas et al., 2010). In our setting, two participants play identical roles in eye-to-eye communication; therefore, the resonance through inter-brain closed loop might occur in the homologous regions. However, the inter-brain effect may also occur between non-homologous regions. To explore this possibility, an ROI analysis based on the precise parcellation of human cerebral cortex in human connectome project (HCP) may be the most suitable (Glasser et al., 2016). Future studies adapting this method could reveal the mechanism underlying the means by which two brains are wired through an eye-to-eye communication without any conscious awareness.

Summary

In the present hyperscanning fMRI study, we focused on real-time mutual interaction during eye contact. The open-and-close timing of the attentional window, defined by eye-blinks, was entrained to that of the counterpart during real-time mutual interaction. Our findings indicate that the social interaction is nonlinear, and the influence from the partner might be amplified by the nonlinearity during the real-time interaction. Corresponding with the nonlinearly amplified behavioral coordination, real-time interaction during eye contact was found to be mediated by the amplified activation of the cerebellum and the cingulate motor cortex.; this was accompanied by enhanced connectivity within the limbic mirror system. These findings underscore the notion that real-time eye contact generates an emergent property of

724 shared attention, which is mediated by a cerebello–cerebral network inclusive of the limbic
725 mirror system.
726
727

728 **Figures**

729

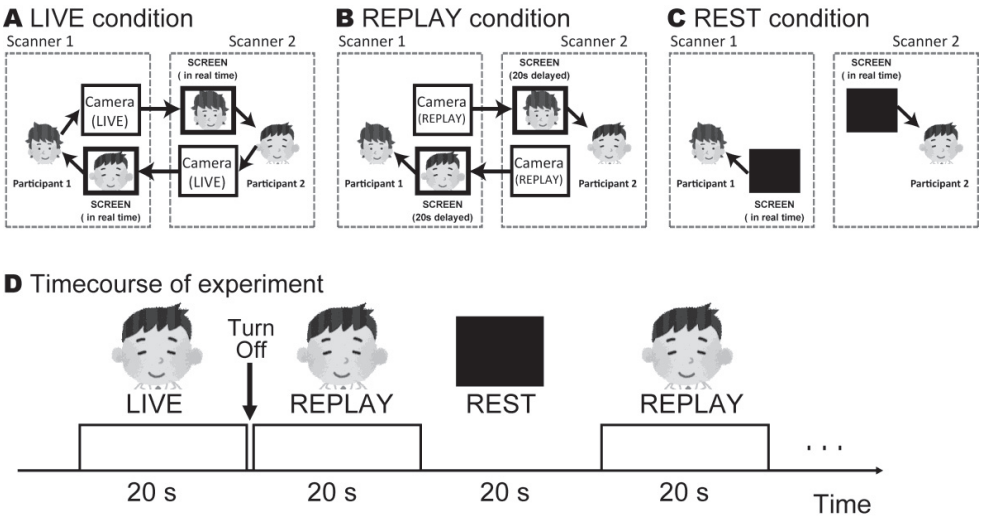

730

731

732 Figure 1. Experimental setup. (A) LIVE condition: The face of Participant 1 is projected on the

733 screen of Participant 2 in real-time and vice versa, allowing mutual exchange of information.

734 (B) REPLAY condition: The picture is projected on the screen with a 20-s delay, therefore,

735 there is no mutual interaction between participants in real-time. (C) REST condition (baseline):

736 No image is presented on the black screen. (D) Sequence of presentation of the experimental

737 conditions.

738

739

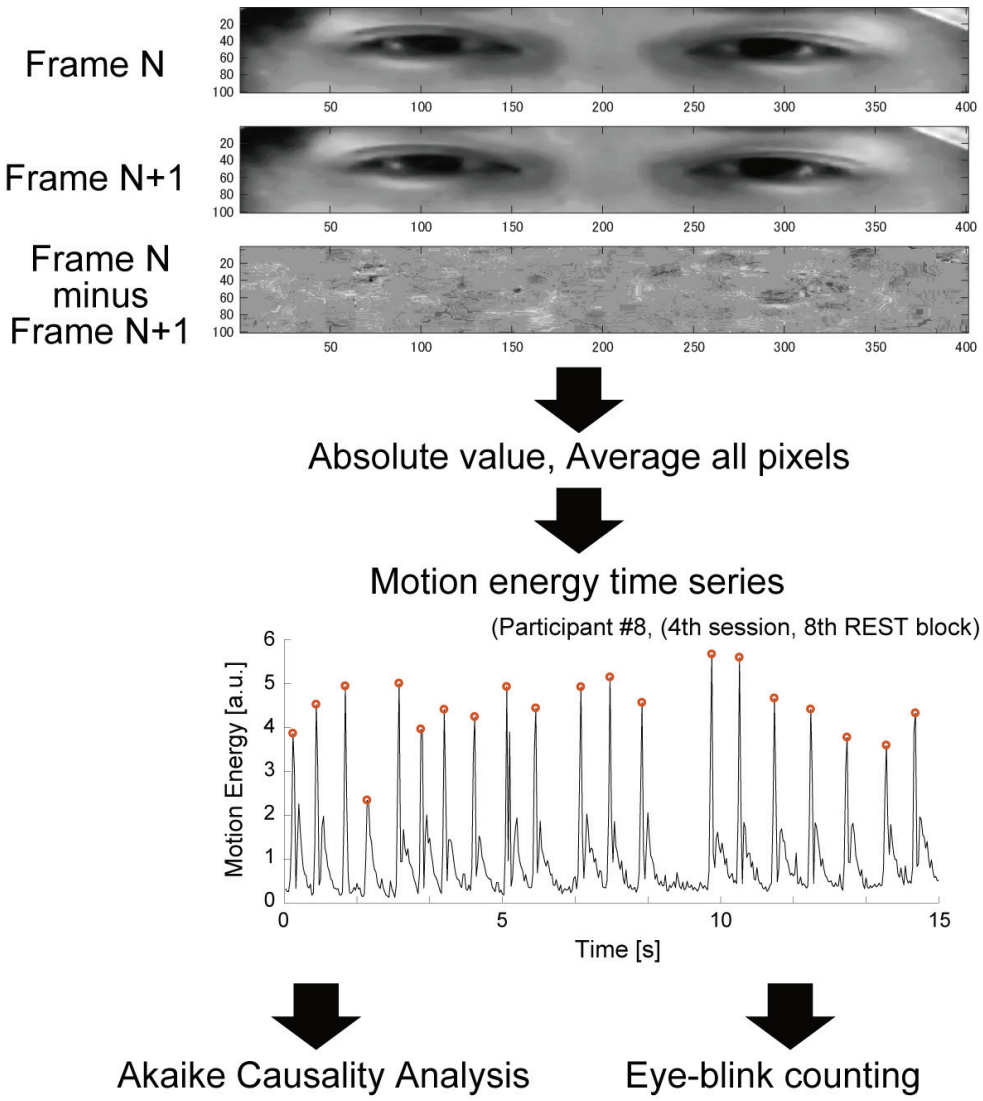

740

741 Figure 2. Evaluation of the motion energy time-series representing eye-blinks. The red-dots

742 indicate the timing of the detected eye-blink.

743

744

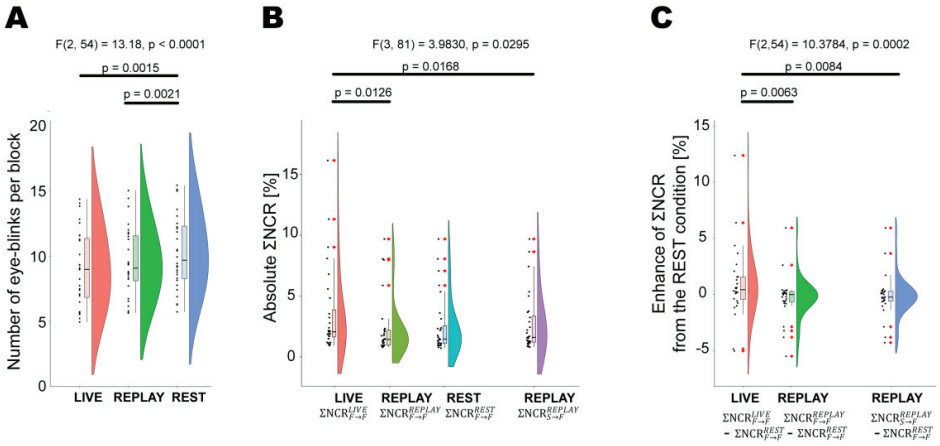

745

746 Figure 3. Behavioral analysis. (A) The number of eye-blinks per block. We omitted the first 5 s
747 of each block because of instability of the recorded video induced by task switching; the number
748 of eye blinks was therefore calculated based on the succeeding 15 s. Each dot represents a data
749 point. In the boxplot, the line dividing the box represents the median of the data, the ends
750 represent the upper/lower quartiles, and the extreme lines represent the highest and lowest
751 values excluding outliers. (B) ΣNCR values. The integral of the Noise Contribution Ratio
752 (NCR) of each condition across the whole frequency range was calculated. $\Sigma\mathrm{NCR}_{F\to F}^{LIVE}$ is the
753 ΣNCR from the time-series of the participant's facial movement to that of the partner during the
754 LIVE condition. $\Sigma\mathrm{NCR}_{F\to F}^{REPLAY}$ is the ΣNCR from the time-series of the participant's facial
755 movement to that of the partner during the REPLAY condition. $\Sigma\mathrm{NCR}_{F\to F}^{REST}$ is the ΣNCR from
756 the time-series of the participant's facial movement to that of the partner during the REST
757 condition. $\Sigma\mathrm{NCR}_{S\to F}^{REPLAY}$ is the ΣNCR from the time-series from the participant's delayed facial
758 movement on the screen to the partner's time-series during the REPLAY condition. (C)
759 Enhanced ΣNCR values from the REST condition.

760

761

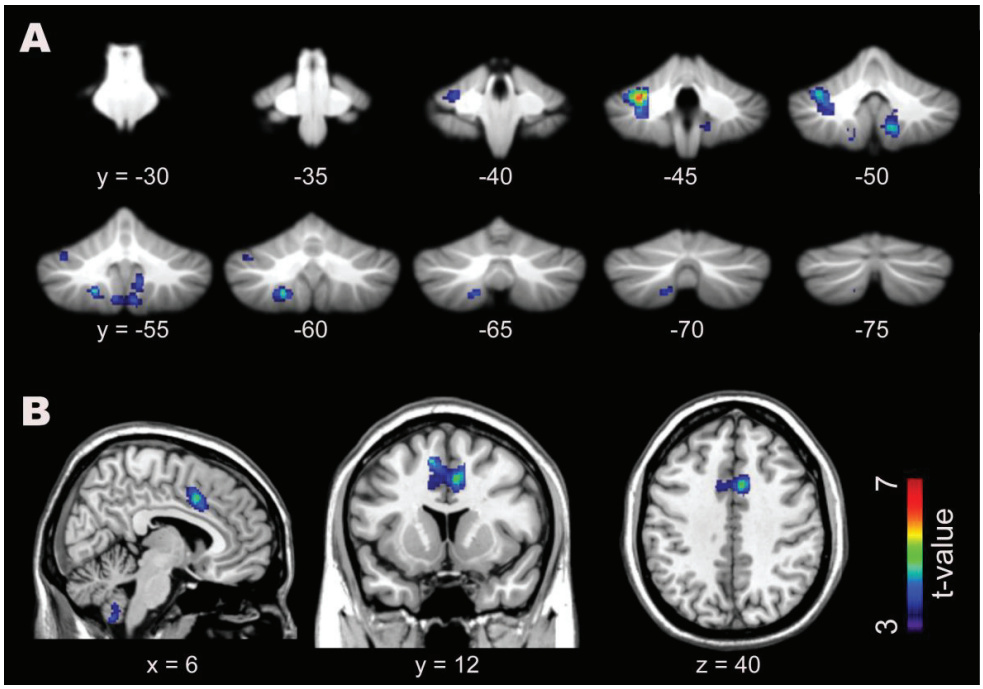

762

763 Figure 4. Brain regions exhibiting significantly greater activation in the LIVE condition than in
764 the REPLAY condition. A, Cerebellar activation is overlaid on the coronal planes of the SUIT
765 template (Diedrichsen, 2006; Diedrichsen et al., 2009). B, The activation in the anterior
766 cingulate cortex (ACC) is superimposed on the T1-weighted high resolution anatomical MRI
767 normalized to the MNI template space in the sagittal (left), coronal (middle), and transaxial
768 (right) planes that crossed at (6, 12, 30) in the MNI coordinate system (mm). MNI: Montreal
769 Neurological Institute; SUIT: spatially unbiased infratentorial template.

770

771

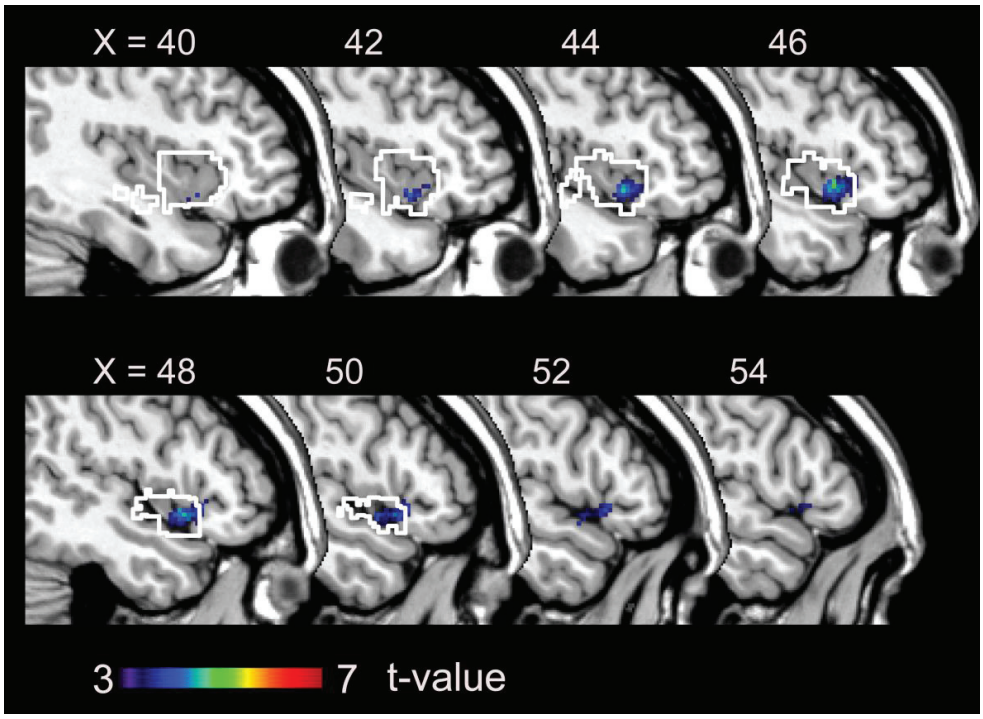

772

773 Figure 5. Regions exhibiting greater effective connectivity from the ACC in the LIVE
774 condition than in the REPLAY condition. The area outlined in white is the dorsal AIC
775 (Chang et al., 2013). X indicates the MNI coordinates (mm). ACC: anterior cingulate
776 cortex; AIC: anterior insular cortex; MNI: Montreal Neurological Institute.

777

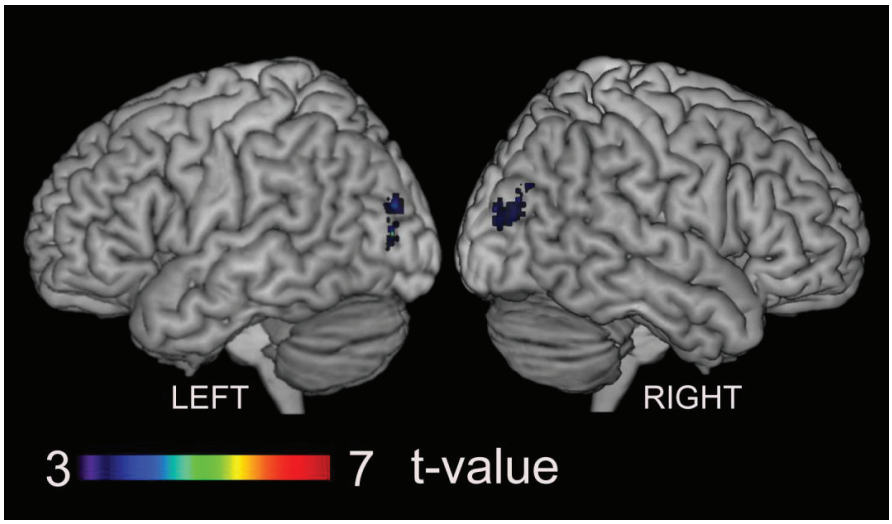

Figure 6. Regions exhibiting greater inter-brain synchronization during the LIVE condition than the REPLAY condition. These areas are superimposed on a surface-rendered high-resolution anatomical MRI normalized to the MNI template viewed from the left and right. MRI: Magnetic resonance imaging; MNI: Montreal Neurological Institute.

Tables

Table 1. Statistical analysis.

Statistics Table									
Location		Data Type	Data structure	Type of test	Multiple comparison correction	Program	Statistics	p-values	Power / Confidence interval
Manuscript	Figure								
a	3A	Number of eye blinks	Normal distribution	One-way repeated ANOVA	--	R	F(2,54) =13.1814	**p<0.0001**	η_g^2 = 0.03540
b		Number of eye blinks	Normal distribution	t-test (Post-hoc test, LIVE vs REST)	Bonferroni	R	T(27)=3.9464	**p=0.0015**	mean = -1.2757 (-1.9389 to -0.6124)
c		Number of eye blinks	Normal distribution	t-test (Post-hoc test, REPLAY vs REST)	Bonferroni	R	T(27)=3.8499	**p=0.0021**	mean = -0.7946 (-1.2182 to -0.3711)
d		Number of eye blinks	Normal distribution	t-test (Post-hoc test, LIVE vs REPLAY)	Bonferroni	R	T(27) = 2.3522,	p=0.0786	mean = -0.4810 (-0.9006 to -0.0614)
e	3B	Absolute ΣNCR	Normal distribution	One-way repeated ANOVA	--	R	F(3,81)=3.9830	**p=0.0295**	η_g^2 = 0.03236
f		Absolute ΣNCR	Normal distribution	Paired t-test (Post-hoc test, LIVEFF vs REPLAYFF)	Bonferroni	R	T(27)=3.406	**p = 0.0126**	mean = 1.2294 (0.4888 to 1.9700)
g		Absolute ΣNCR	Normal distribution	Paired t-test (Post-hoc test, LIVEFF vs RESTFF)	Bonferroni	R	T(27)=1.4598	p = 0.9354	mean = 0.8888 (-0.3604 to 2.1379)
h		Absolute ΣNCR	Normal distribution	Paired t-test (Post-hoc test, LIVEFF vs REPLAYSF)	Bonferroni	R	T(27)=3.2934	**p = 0.0168**	mean = 1.0455 (0.3941 to 1.6969)
i		Absolute ΣNCR	Normal distribution	Paired t-test (Post-hoc test, REPLAYFF vs RESTFF	Bonferroni	R	T(27)=0.9065	p = 1.0000	mean = -0.3406 (-1.1116 to 0.4304)
j		Absolute ΣNCR	Normal distribution	Paired t-test (Post-hoc test, REPLAYFF vs REPLAYSF	Bonferroni	R	T(27)=1.2083	p = 1.0000	mean = -0.1838 (-0.4960 to 0.1284)
k		Absolute ΣNCR	Normal distribution	Paired t-test (Post-hoc test, RESTFF vs REPLAYSF	Bonferroni	R	T(27)=0.4349	p = 1.0000	mean = 0.1568 (-0.5829 to 0.8965)
l		Absolute ΣNCR	Normal distribution	One-way repeated ANOVA	--	R	F(3,69)=4.3334	**p=0.0074**	η_g^2= 0.0785
m		Absolute ΣNCR	Normal distribution	Paired t-test (Post-hoc test, LIVEFF vs REPLAYFF)	Bonferroni	R	T(23)=3.0965	**p=0.0306**	mean = 1.0291 (0.3416 to 1.7165)
n		Absolute ΣNCR	Normal distribution	Paired t-test (Post-hoc test, LIVEFF vs RESTFF)	Bonferroni	R	T(23)=1.0783	p=1.0000	mean = 0.4588 (-0.4214 to 1.3390)
o		Absolute ΣNCR	Normal distribution	Paired t-test (Post-hoc test, LIVEFF vs REPLAYSF)	Bonferroni	R	T(23)=3.0779	**p=0.0318**	mean = 0.7771 (0.2548 to 1.2994)
p		Absolute ΣNCR	Normal distribution	Paired t-test (Post-hoc test, REPLAYFF vs RESTFF	Bonferroni	R	T(23)=1.9902	p=1.0000	mean = -0.5702 (-1.1630 to 0.0225)
q		Absolute ΣNCR	Normal distribution	Paired t-test (Post-hoc test, REPLAYFF vs REPLAYSF	Bonferroni	R	T(23)=1.4744	p=0.9234	mean = -0.2519 (-0.6054 to 0.1015)
r		Absolute ΣNCR	Normal distribution	Paired t-test (Post-hoc test, REPLAYFF vs REPLAYSF	Bonferroni	R	T(23)=1.1336	p=1.0000	mean = 0.3183 (-0.2626 to 0.8992)
s	3C	RelativeΣNCR	Normal distribution	Paired t-test (Post-hoc test, RESTFF vs REPLAYSF	Bonferroni	R	F(2,54)=10.3784	**p = 0.0002**	η_g^2= 0.0483
t		RelativeΣNCR	Normal distribution	Paired t-test (Post-hoc test, LIVEFF vs REPLAYFF	Bonferroni	R	T(27)=3.4061	**p = 0.0063**	mean = 1.2294 (0.4888 to 1.9700)
u		RelativeΣNCR	Normal distribution	Paired t-test (Post-hoc test, LIVEFF vs REPLAYSF	Bonferroni	R	T(27)=3.2934	**p = 0.0084**	mean = 1.0455 (0.3941 to 1.6969)
v		RelativeΣNCR	Normal distribution	Paired t-test (Post-hoc test, REPLAYFF vs RESTSF	Bonferroni	R	T(27)=1.2083	p = 0.7122	mean = -0.1838 (-0.4960 to 0.1284)
w		RelativeΣNCR	Normal distribution	Paired t-test (Post-hoc test, RESTFF vs REPLAYSF	Bonferroni	R	F(2,40)=7.9233	**p=0.0013**	η_g^2= 0.1330
x		RelativeΣNCR	Normal distribution	Paired t-test (Post-hoc test, LIVEFF vs REPLAYFF	Bonferroni	R	T(20)=2.8343	**p=0.0306**	mean = 7805 (0.0102 to 0.0250)
y		RelativeΣNCR	Normal distribution	Paired t-test (Post-hoc test, LIVEFF vs REPLAYSF	Bonferroni	R	T(20)=2.9034	**p=0.0264**	mean = 0.8362 (0.0088 to 0.0167)
z		RelativeΣNCR	Normal distribution	Paired t-test (Post-hoc test, REPLAYFF vs RESTSF	Bonferroni	R	T(20)=0.6790	p=1.0000	mean = 0.0558 (-0.1156 to 0.2271)
aa	4	fMRI (BOLD activation)	Normal distribution	Paired t-test (LIVE > REPLAY)	Random effect model at cluster-level inference	SPM	--	--	--
bb		fMRI (BOLD activation)	No assumption	Paired t-test (LIVE > REPLAY)	Nonparametric permutation test at cluster-level inference	SnPM	--	--	--
cc	5	fMRI (PPI value)	Normal distribution	Paired t-test (LIVE > REPLAY)	Random effect model at cluster-level inference	SPM	--	--	--
dd		fMRI (PPI value)	No assumption	Paired t-test (LIVE > REPLAY)	Nonparametric permutation test at cluster-level inference	SnPM	--	--	--
ee	6	fMRI (Normalized inter-brain sync)	Normal distribution	Paired t-test (LIVE > REPLAY)	Random effect model at cluster-level inference	SPM	--	--	--
ff		fMRI (Normalized inter-brain sync)	No assumption	Paired t-test (LIVE > REPLAY)	Nonparametric permutation test at cluster-level inference	SnPM	--	--	--

Table 2. Regions exhibiting greater activation in the LIVE condition than in the REPLAY condition. The p-values satisfying the statistical threshold ($p<0.05$) after correcting for multiple comparisons (pFWE) are emphasized using a bold type-face. FWE: family-wise error.

Cluster level inference			Peak level inference			MNI coordinates					
P_{FWE}		Cluster size mm^3	P_{FWE}		T-value				Side	Location	Probability
SPM	SnPM		SPM	SnPM		X	Y	Z			
0.015	**0.025**	2616	0.960	0.443	3.848	-40	-60	-30	L	Cerebellum	Lobule VIIa crus I (Hem) (99%)
			0.006	0.001	6.734	-28	-46	-30	L	Cerebellum	Lobule VI (Hem) (85%)
			0.642	0.195	4.406	-28	-44	-44	L	Cerebellum	
0.010	**0.022**	2880	0.408	0.111	4.720	-18	-60	-52	L	Cerebellum	Lobule VIIIb (Hem) (68%)
			0.846	--	4.119	-6	-54	-54	L	Cerebellum	Lobule IX (Hem) (80%)
			0.954	--	3.870	-14	-52	-52	L	Cerebellum	Lobule IX (Hem) (67%)
			0.815	0.283	4.169	6	-56	-56	R	Cerebellum	Lobule IX (Hem) (86%)
			0.495	0.139	4.598	12	-50	-50	R	Cerebellum	Lobule IX (Hem) (87%)
0.002	**0.014**	4176	0.274	0.069	4.945	-8	10	50	L	Pre-SMA	
			0.986	0.532	3.702	-10	10	38	L	ACC	
			0.274	0.069	4.945	6	12	40	R	ACC	
0.056	**0.040**	1824	0.227	0.055	5.044	-8	-46	-22	L	Cerebellum	
			0.463	0.127	4.641	0	-56	-26	R	Cerebellum	Fastigii Nucleus (37%)
			0.471	0.130	4.630	14	-52	-30	R	Cerebellum	

ACC, Anterior cingulate cortex; Pre-SMA, Pre-supplementary motor area; MNI, Montreal Neurological Institute; Hem, Hemisphere

798

799 **T**able 3. Regions exhibiting enhanced effective connectivity from the anterior cingulate
800 cortex (ACC) in the LIVE condition. The p-values satisfying the statistical threshold
801 ($p<0.05$) after correcting for multiple comparisons (pFWE) are emphasized using a bold
802 type-face. FEW: family-wise error

Cluster level inference			Peak level inference			MNI coordinates					
P_{FWE}		Cluster size mm^3	P_{FWE}		T-value	X	Y	Z	Side	Location	Probability
SPM	SnPM		SPM	SnPM							
0.000	0.0824	1208	0.868	0.378	5.063	46	14	-6	R	Insular	
			1.000	1.000	3.545	54	14	-4	R	IFG	BA44 (21%)
			1.000	--	4.156	50	20	-4	R	IFGOr	BA45 (31%)

IFG, Inferior frontal gyrus; IFGOr, Inferior frontal gyrus (pars opercularis); Montreal Neurological Institute; BA, Brodmann area

803

804

Table 4. The regions exhibiting enhanced inter-brain synchronization in the LIVE condition compared to REPLAY condition. The p-values satisfying the statistical threshold ($p<0.05$) after correcting for multiple comparisons (pFWE) are emphasized using a bold type-face.

Cluster level inference			Peak level inference			MNI coordinates					
P_{FWE}		Cluster size mm^3	P_{FWE}		T-value				Side	Location	Probability
SPM	SnPM		SPM	SnPM		X	Y	Z			
0.001	0.2258	1088	0.999	0.829	5.753	-26	-82	4	L		
			1.000	0.999	4.695	-34	-78	4	L	MOG	
			1.000	0.999	4.628	-28	-86	22	L	MOG	
0.007	0.2852	880	1.000	0.998	4.739	28	-76	24	R	MOG	
			1.000	1.000	3.983	38	-80	16	R	MOG	
			1.000	1.000	3.827	34	-88	18	R	MOG	hOc4lp (35.4%)

MOG, Middle Occipital Gyrus; Montreal Neurological Institute

811 References

812

813 Akaike H (1968) On the use of a linear model for the identification of feedback systems. Ann Inst
814 Stat Math 20:425-439.
815 Allen G, Buxton RB, Wong EC, Courchesne E (1997) Attentional activation of the cerebellum
816 independent of motor involvement. Science 275:1940-1943.
817 Allen M, Poggiali D, Whitaker K, Marshall TR, Kievit R (2018) Raincloud plots: a
818 multi-platform tool for robust data visualization. PeerJ Preprints 6:e27137v1
819 Astafiev S V., Stanley CM, Shulman GL, Corbetta M (2004) Extrastriate body area in human
820 occipital cortex responds to the performance of motor actions. Nat Neurosci 7:542-548.
821 Bernieri F, Rosenthal R (1991) Interpersonal coordination: Behavior matching and interactional
822 synchrony. In: Fundamentals of nonverbal behavior (Feldman RS, Rime B, eds), pp
823 401-432. New York: Cambridge University Press.
824 Blakemore SJ, Boyer P, Pachot-Clouard M, Meltzoff A, Segebarth C, Decety J (2003) The
825 detection of contingency and animacy from simple animations in the human brain. Cereb
826 Cortex 13:837-844.
827 Blakemore SJ, Sirigu A (2003) Action prediction in the cerebellum and in the parietal lobe. Exp
828 Brain Res 153:239-245.
829 Brázdil M, Kuba R, Rektor I (2006) Rostral cingulate motor area and paroxysmal alien hand
830 syndrome. J Neurol Neurosurg Psychiatry 77:992-993.
831 Buckner RL, Krienen FM, Castellanos A, Diaz JC, Yeo BTT (2011) The organization of the
832 human cerebellum estimated by intrinsic functional connectivity. J Neurophysiol
833 106:2322-2345.
834 Calder AJ, Lawrence AD, Keane J, Scott SK, Owen AM, Christoffels I, Young AW (2002)
835 Reading the mind from eye gaze. Neuropsychologia 40:1129-1138.
836 Caspers S, Zilles K, Laird AR, Eickhoff SB (2010) ALE meta-analysis of action observation and
837 imitation in the human brain. Neuroimage 50:1148-1167.
838 Cattaneo L, Rizzolatti G (2009) The mirror neuron system. Arch Neurol 66:557-560.
839 Chang LJ, Yarkoni T, Khaw MW, Sanfey AG (2013) Decoding the role of the insula in human
840 cognition: Functional parcellation and large-scale reverse inference. Cereb Cortex
841 23:739-749.
842 Chartrand TL, Van Baaren RB (2009) Human mimicry. Adv Exp Soc Psychol 41:219-274.
843 Conty L, N'Diaye K, Tijus C, George N (2007) When eye creates the contact! ERP evidence for
844 early dissociation between direct and averted gaze motion processing. Neuropsychologia
845 45:3024-3037.

846 Craig AD (2009) How do you feel - now? The anterior insula and human awareness. Nat Rev
847 Neurosci 10:59-70.
848 Deiber MP, Ibañez V, Sadato N, Hallett M (1996) Cerebral structures participating in motor
849 preparation in humans: a positron emission tomography study. J Neurophysiol 75:233-247.
850 Diedrichsen J (2006) A spatially unbiased atlas template of the human cerebellum. Neuroimage
851 33:127–138.
852 Diedrichsen J, Balsters JH, Flavell J, Cussans E, Ramnani N (2009) A probabilistic MR atlas of
853 the human cerebellum. Neuroimage 46:39–46.
854 Dosenbach NUF, Visscher KM, Palmer ED, Miezin FM, Wenger KK, Kang HC, Burgund ED,
855 Grimes AL, Schlaggar BL, Petersen SE (2006) A core system for the implementation of
856 task sets. Neuron 50:799-812.
857 Dumas G, Nadel J, Soussignan R, Martinerie J, Garnero L (2010) Inter-brain synchronization
858 during social interaction. PLoS One 5(8): e12166.
859 Eickhoff SB, Stephan KE, Mohlberg H, Grefkes C, Fink GR, Amunts K, Zilles K (2005) A new
860 SPM toolbox for combining probabilistic cytoarchitectonic maps and functional imaging
861 data. Neuroimage 25:1325-1335.
862 Eklund A, Nichols TE, Knutsson H (2016) Cluster failure: Why fMRI inferences for spatial extent
863 have inflated false-positive rates. Proc Natl Acad Sci U S A 113:7900-7905.
864 Emery N (2000) The eyes have it: The neuroethology, function and evolution of social gaze.
865 Neurosci Biobehav Rev 24:581-604.
866 Fabbri-Destro M, Rizzolatti G (2008) Mirror neurons and mirror systems in monkeys and humans.
867 Physiology 23:171-179.
868 Fair D, Schlaggar B, Cohen A, Miezin F, Dosenbach NUF, Wenger KK, Fox MD, Snyder AZ,
869 Raichle ME, Petersen SE (2007) A method for using blocked and event-related fMRI data
870 to study “resting state” functional connectivity. Neuroimage 35:396–405.
871 Farroni T, Csibra G, Simion F, Johnson MH (2002) Eye contact detection in humans from birth.
872 Proc Natl Acad Sci U S A 99:9602-9605.
873 Flandin G, Friston KJ (2017) Analysis of family-wise error rates in statistical parametric mapping
874 using random field theory. Hum Brain Mapp 00:0-2 Available at:
875 http://doi.wiley.com/10.1002/hbm.23839.
876 Franz VH, Loftus GR (2012) Standard errors and confidence intervals in within-subjects designs:
877 Generalizing Loftus and Masson (1994) and avoiding the biases of alternative accounts.
878 Psychon Bull Rev 19:395–404.
879 Friston KJ, Buechel C, Fink GR, Morris J, Rolls E, Dolan RJ (1997) Psychophysiological and
880 modulatory interactions in neuroimaging. Neuroimage 6:218-229.
881 Friston KJ, Glaser DE, Henson RN, Kiebel S, Phillips C, Ashburner J (2002) Classical and

882 Bayesian inference in neuroimaging: applications. Neuroimage 16:484-512.
883 Friston KJ, Holmes A, Poline JB, Price CJ, Frith CD (1996) Detecting activations in PET and
884 fMRI: levels of inference and power. Neuroimage 4:223-235.
885 Friston KJ, Holmes AP, Worsley KJ (1999) How many subjects constitute a study? Neuroimage
886 10:1-5.
887 Froese T, Fuchs T (2012) The extended body: A case study in the neurophenomenology of social
888 interaction. Phenomenology and the Cognitive Sciences 11(2): 205-235.
889 George N, Driver J, Dolan RJ (2001) Seen gaze-direction modulates fusiform activity and its
890 coupling with other brain areas during face processing. Neuroimage 13:1102-1112.
891 Gergely G (2001) The obscure object of desire: "Nearly, but Clearly Not, Like Me": Contingency
892 preference in normal children versus children with autism. Bull Menninger Clin
893 65:411-426.
894 Gergely G, Watson JS (1999) Early socio–emotional development: Contingency perception and
895 the social-biofeedback model. In P. Rochat (Ed.), Early social cognition: Understanding
896 others in the first months of life (pp. 101-136). Mahwah, NJ, US: Lawrence Erlbaum
897 Associates Publishers.
898 Ghaziri J, Tucholka A, Girard G, Houde J-C, Boucher O, Gilbert G, Descoteaux M, Lippe S,
899 Rainville P, Nguyen DK (2015) The corticocortical structural connectivity of the human
900 insula. Cereb Cortex 27(2):1-13.
901 Giraud AL, Poeppel D (2012) Cortical oscillations and speech processing: Emerging
902 computational principles and operations. Nat Neurosci 15:511-517.
903 Glasser M, Coalson T, Robinson E, Hacker C, Harwell J, Yacoub E, Ugurbil K, Andersson J,
904 Beckmann C, Jenkinson M, Smith S, Van Essen D (2016) A multi-modal parcellation of
905 human cerebral cortex. Nature 536: 171-178.
906 Goldstein MH, King AP, West MJ (2003) Social interaction shapes babbling: testing parallels
907 between birdsong and speech. Proc Natl Acad Sci U S A 100:8030-8035.
908 Habas C (2010) Functional connectivity of the human rostral and caudal cingulate motor areas in
909 the brain resting state at 3T. Neuroradiology 52:47-59.
910 Haken H (1983) Advanced synergetics: Instability hierarchies of self-organizing systems and
911 devices. Berlin: Springer-Verlag.
912 Hall A (1945) The origin and purposes of blinking. Bri J Opthalmol 29:445-467.
913 Hari R, Kujala M (2009) Brain basis of human social interaction: from concepts to brain imaging.
914 Physiol Rev 89:453-479.
915 Herrmann A (2010) The interaction of eye blinks and other prosodic cues in German Sign
916 Language. Sign Lang Linguist 13:3-39.
917 Hietanen JK, Leppänen JM, Peltola MJ, Linna-Aho K, Ruuhiala HJ (2008) Seeing direct and

averted gaze activates the approach-avoidance motivational brain systems. Neuropsychologia 46:2423-2430.

Honey GD, Pomarol-Clotet E, Corlett PR, Honey RAE, Mckenna PJ, Bullmore ET, Fletcher PC (2005) Functional dysconnectivity in schizophrenia associated with attentional modulation of motor function. Brain 128:2597-2611.

Imamizu H, Miyauchi S, Tamada T, Sasaki Y, Takino R, Putz B, Yoshioka T, Kawato M (2000) Human cerebellar activity reflecting an acquired internal model of a new tool. Nature 403:192-195.

Kampe KKW, Frith CD, Frith U (2003) "Hey John": signals conveying communicative intention toward the self activate brain regions associated with "mentalizing," regardless of modality. J Neurosci 23:5258-5263.

Kawashima R, Sugiura M, Kato T, Nakamura A, Hatano K, Ito K, Fukuda H, Kojima S, Nakamura K (1999) The human amygdala plays an important role in gaze monitoring. Brain 122:779-783.

Koike T, Tanabe HC, Sadato N (2015) Hyperscanning neuroimaging technique to reveal the "two-in-one" system in social interactions. Neuroscience Research 90:25-32.

Koike T, Tanabe HC, Okazaki S, Nakagawa E, Sasaki AT, Shimada K, Sugawara SK, Takahashi HK, Yoshihara K, Bosch-Bayard J, Sadato N (2016) Neural substrates of shared attention as social memory: A hyperscanning functional magnetic resonance imaging study. Neuroimage 125:401-412.

Kuhl PK, Tsao F-M, Liu H-M (2003) Foreign-language experience in infancy: effects of short-term exposure and social interaction on phonetic learning. Proc Natl Acad Sci U S A 100:9096-9101.

Lamm C, Singer T (2010) The role of anterior insular cortex in social emotions. Brain Struct Funct 214:579-559.

Leong V, Byrne E, Clackson K, Georgieva S, Lam S, Wass S (2017) Speaker gaze increases information coupling between infant and adult brains. Proc Natl Acad Sci 114:13290-13295.

Lingnau A, Downing PE (2015) The lateral occipitotemporal cortex in action. Trends Cogn Sci 19:268-277.

Margulies DS, Kelly CAM, Uddin LQ, Biswal BB, Castellanos FX, Milham MP (2007) Mapping the functional connectivity of anterior cingulate cortex. Neuroimage 37:579-588.

Matsuzawa M, Matsuo K, Sugio T, Kato C, Nakai T (2005) Temporal relationship between action and visual outcome modulates brain activation: an fMRI study. Magn Reson Med Sci 4:115-121.

McLaren DG, Ries ML, Xu G, Johnson SC (2012) A generalized form of context-dependent

psychophysiological interactions (gPPI): A comparison to standard approaches. Neuroimage 61:1277-1286.

Medford N, Critchley HD (2010) Conjoint activity of anterior insular and anterior cingulate cortex: awareness and response. Brain Struct Funct 214:535-549.

Meltzoff AN (2005) Imitation and other minds: The "Like Me" hypothesis. In: Perspectives on imitation: from neuroscience to social science (Hurley S, Chater N, eds), pp 55-77. Cambridge, MA: MIT Press.

Moeller S, Yacoub E, Olman CA, Auerbach E, Strupp J, Harel N, Uğurbil K (2010) Multiband multislice GE-EPI at 7 tesla, with 16-fold acceleration using partial parallel imaging with application to high spatial and temporal whole-brain FMRI. Magn Reson Med 63:1144-1153.

Morita T, Tanabe HC, Sasaki AT, Shimada K, Kakigi R, Sadato N (2014) The anterior insular and anterior cingulate cortices in emotional processing for self-face recognition. Soc Cogn Affect Neurosci 9:570-579.

Mundy P, Sigman M (1989) The theoretical implications of joint-attention deficits in autism. Dev Psychopathol 1:173-183.

Murray L, Trevarthen C (1985) Emotional regulation of interaction between 2-month-olds and their mothers. In: Social perception in infants (Field TM, Fox NA, eds), pp 177-197. Norwood.

Nadel J (2002) Imitation and imitation recognition: Functional use in preverbal infants and nonverbal children with autism. In: The imitative mind Development evolution and brain (Meltzoff AN, Prinz W, eds), pp 42-62. Cambridge University Press.

Nakano T, Kitazawa S (2010) Eyeblink entrainment at breakpoints of speech. Exp Brain Res 205:577-581.

Nicolis G, Prigogine IS (1977) Self-organization in nonequilibrium systems: from dissipative structures to order through fluctuations. New York: Wiley.

Noy L, Dekel E, Alon U (2011) The mirror game as a paradigm for studying the dynamics of two people improvising motion together. Proc Natl Acad Sci U S A 108:20947-20952.

Okazaki S, Hirotani M, Koike T, Bosch-Bayard J, Takahashi HK, Hashiguchi M, Sadato N (2015) Unintentional interpersonal synchronization represented as a reciprocal visuo-postural feedback system: a multivariate autoregressive modeling approach. PLoS One 10:e0137126.

Olejnik S, Algina J (2003) Generalized Eta and Omega Squared Statistics: Measures of Effect Size for Some Common Research Designs. Psychol Methods 8:434–447.

Oldfield RC (1971) The assessment and analysis of handedness: the Edinburgh inventory. Neuropsychologia 9:97-113.

990 Orchard LN, Stern JA (1991) Blinks as an index of cognitive activity during reading. Integr
991 Physiol Behav Sci 26:108-116.
992 Oosterhof NN, Tipper SP, Downing PE (2013) Crossmodal and action-specific: neuroimaging the
993 human mirror neuron system. Trends Cogn Sci 17:311-318.
994 Orlov T, Makin TR, Zohary E (2010) Topographic representation of the human body in the
995 occipitotemporal cortex. Neuron 68:586-600.
996 Oullier O, de Guzman GC, Jantzen KJ, Lagarde J, Kelso JA (2008) Social coordination dynamics:
997 measuring human bonding. Soc Neurosci 3:178-192.
998 Ozaki (2012) Time-series Modeling of Neuroscience Data. FL: CRC press.
999 Pageler NM, Menon V, Merin NM, Eliez S, Brown WE, Reiss AL (2003) Effect of head
1000 orientation on gaze processing in fusiform gyrus and superior temporal sulcus. Neuroimage
1001 20:318-329.
1002 Paus T (2001) Primate anterior cingulate cortex: where motor control, drive and cognition
1003 interface. Nat Rev Neurosci 2:417-424.
1004 Paus T, Petrides M, Evans AC, Meyer E (1993) Role of the human anterior cingulate cortex in the
1005 control of oculomotor, manual, and speech responses: a positron emission tomography
1006 study. J Neurophysiol 70:453-469.
1007 Pelphrey K, Viola R, McCarthy G (2004) When strangers pass: Processing of mutual and averted
1008 social gaze in the superior temporal sulcus. Psychol Sci 15:598-603.
1009 Picard N, Strick PL (1996) Motor areas of the median wall: a review of their location and
1010 functional activation. Cereb Cortex 6:342-353.
1011 Ponder E, Kennedy WP (1927) On the act of blinking. Q J Exp Physiol 18:89-110.
1012 Prochazkova E, Kret ME (2017) Connecting minds and sharing emotions through mimicry: A
1013 neurocognitive model of emotional contagion. Neurosci Biobehav Rev 80:99-114.
1014 Riedel MC, Ray KL, Dick AS, Sutherland MT, Hernandez Z, Fox PM, Eickhoff SB, Fox PT,
1015 Laird AR (2015) Meta-analytic connectivity and behavioral parcellation of the human
1016 cerebellum. Neuroimage 117:327-342.
1017 Rochat P (2001) Social contingency detection and infant development. Bull Menn Clin
1018 65:347-360.
1019 Rochat P, Passos-Ferreira C, Salem P (2009) Three Levels of Intersubjectivity in Early
1020 Development. In: Enacting Intersubjectivity. Paving the way for a dialogue between
1021 cognitive science, social cognition and neuroscience (Carassa A, Morganti F, Rivaeds G,
1022 eds), pp173-190. Lugano, Switzerland: Università della Svizzera Italiana.
1023 Rorden C, Brett M (2000) Stereotaxic display of brain lesions. Behavioural Neurology,
1024 12:191-200.
1025 Sato W, Kochiyama T, Yoshikawa S, Naito E, Matsumura M (2004) Enhanced neural activity in

response to dynamic facial expressions of emotion: an fMRI study. Brain Res Cogn Brain Res 20:81-91.

Saito DN, Tanabe HC, Izuma K, Hayashi MJ, Morito Y, Komeda H, Uchiyama H, Kosaka H, Okazawa H, Fujibayashi Y, Sadato N (2010) "Stay tuned": Inter-individual neural synchronization during mutual gaze and joint attention. Front Integr Neurosci 4:1-12.

Schilbach L (2015) Eye to eye, face to face and brain to brain: novel approaches to study the behavioral dynamics and neural mechanisms of social interactions. Curr Opin Behav Sci 3:130-135.

Schilbach L, Wohlschlaeger AM, Kraemer NC, Newen A, Shah NJ, Fink GR, Vogeley K (2006) Being with virtual others: Neural correlates of social interaction. Neuropsychologia 44:718-730.

Schippers MB, Roebroeck A, Renken R, Nanetti L, Keysers C (2010) Mapping the information flow from one brain to another during gestural communication. Proc Natl Acad Sci U S A 107:9388-9393.

Schmahmann JD, Sherman JC (1998) The cerebellar cognitive affective syndrome. Brain 121:561-579.

Schroeder CE, Lakatos P (2009) Low-frequency neuronal oscillations as instruments of sensory selection. Trends Neurosci 32:9-18.

Schweizer TA, Alexander MP, Cusimano M, Stuss DT (2007) Fast and efficient visuotemporal attention requires the cerebellum. Neuropsychologia 45:3068-3074.

Sebanz N, Bekkering H, Knoblich G (2006) Joint action: bodies and minds moving together. Trends Cogn Sci 10:70-76.

Senju A, Johnson MH (2009) The eye contact effect: Mechanisms and development. Trends Cogn Sci 13:127-134.

Singer T, Seymour B, O'Doherty J, Kaube H, Dolan RJ, Frith CD (2004) Empathy for pain involves the affective but not sensory components of pain. Science 303:1157-1162.

Soussignan R, Nadel J, Canet P, Gerardin P (2006) Sensitivity to Social Contingency and Positive Emotion in 2-Month-Olds. Infancy 10:123-144.

Stern JA, Walrath LC, Goldstein R (1984) The endogenous eyeblink. Psychophysiology 21:22-33.

Stevanovic M, Peräkylä A (2015) Experience sharing, emotional reciprocity, and turn-taking. Front Psychol 6:1-7.

Stormark KM, Braarud HC (2004) Infants' sensitivity to social contingency: A "double video" study of face-to-face communication between 2- and 4-month-olds and their mothers. Infant Behav Dev 27:195-203.

Strogatz SH (2003) Sync: The emerging science of spontaneous order. New York: Hyperion.

Tanabe HC, Kosaka H, Saito DN, Koike T, Hayashi MJ, Izuma K, Komeda H, Ishitobi M, Omori

M, Munesue T, Okazawa H, Wada Y, Sadato N (2012) Hard to " tune in ": neural mechanisms of eye contact and joint attention in high-functioning autistic spectrum disorder. Front Hum Neurosci 6:268.

Trillenberg P, Verleger R, Teetzmann A, Wascher E, Wessel K (2004) On the role of the cerebellum in exploiting temporal contingencies: Evidence from response times and preparatory EEG potentials in patients with cerebellar atrophy. Neuropsychologia 42:754-763.

Tzourio-Mazoyer N, Landeau B, Papathanassiou D, Crivello F, Etard O, Delcroix N, Mazoyer B, Joliot M (2002) Automated anatomical labeling of activations in SPM using a macroscopic anatomical parcellation of the MNI MRI single-subject brain. Neuroimage 15:273-289.

VanderWerf F, Brassinga P, Reits D, Aramideh M, Ongerboer de Visser B (2003) Eyelid movements: behavioral studies of blinking in humans under different stimulus conditions. J Neurophysiol 89:2784-2796.

Watanabe K (2013) Teaching as a dynamic phenomenon with interpersonal interactions. Mind, Brain, Educ 7:91-100.

Whitfield-Gabrieli S, Nieto-Castanon A (2012) Conn: A functional connectivity toolbox for correlated and anticorrelated brain networks. Brain Connect 2:125-141.

Wicker B, Keysers C, Plailly J, Royet JP, Gallese V, Rizzolatti G (2003) Both of us disgusted in my insula : the common neural basis of seeing and feeling disgust. Neuron 40:655-664.

Wolpert DM, Doya K, Kawato M (2003) A unifying computational framework for motor control and social interaction. Philos Trans R Soc B Biol Sci 358:593-602.

Wolpert DM, Kawato M (1998) Multiple paired forward and inverse models for motor control. Neural Networks 11:1317-1329.

Zalesky A, Akhlaghi H, Corben LA, Bradshaw JL, Delatycki MB, Storey E, Georgiou-Karistianis N, Egan GF (2014) Cerebello-cerebral connectivity deficits in Friedreich ataxia. Brain Struct Funct 219:969-981.

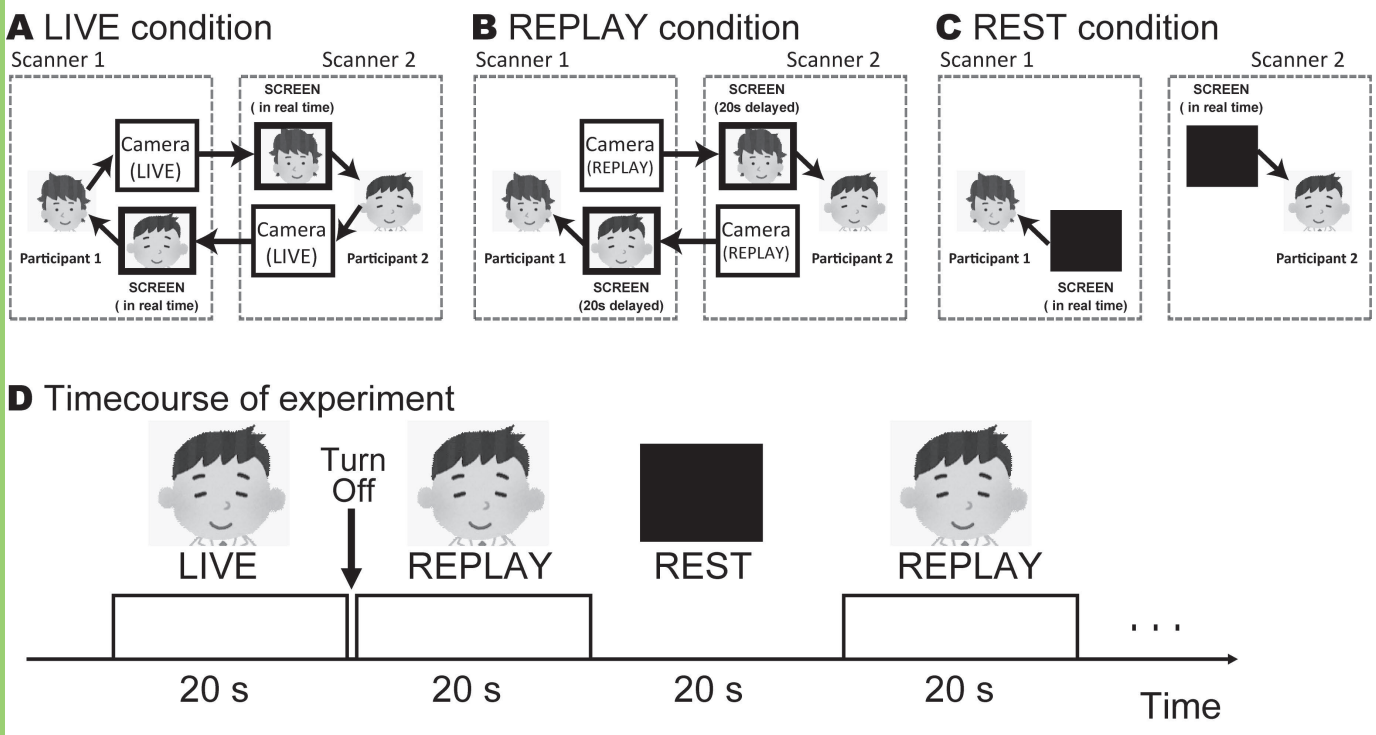

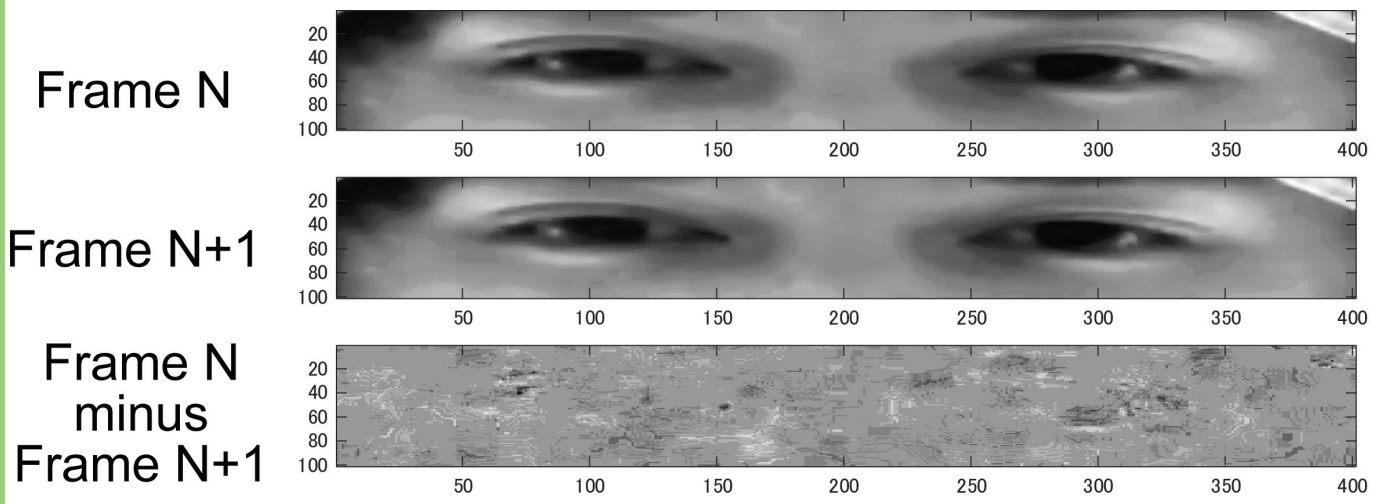

Absolute value, Average all pixels

Motion energy time series

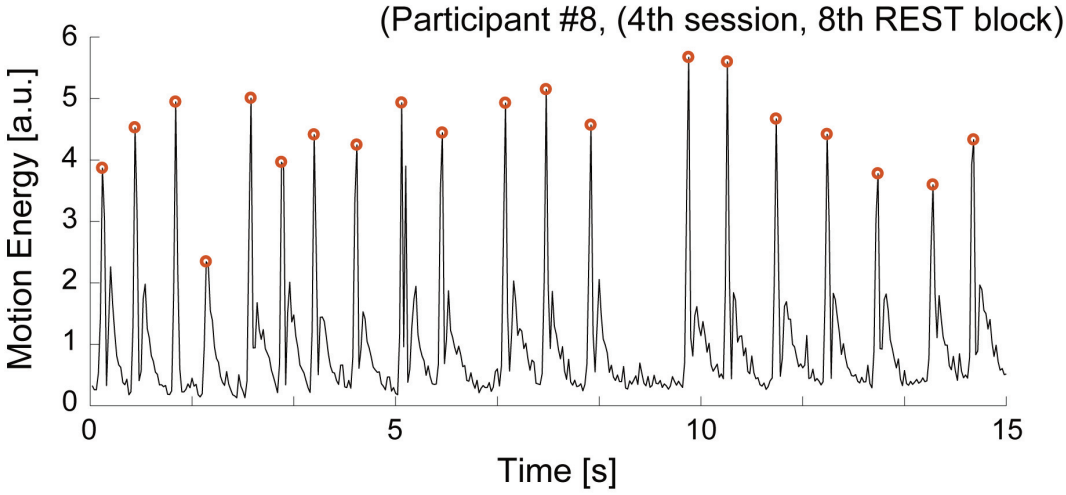

Akaike Causality Analysis

Eye-blink counting

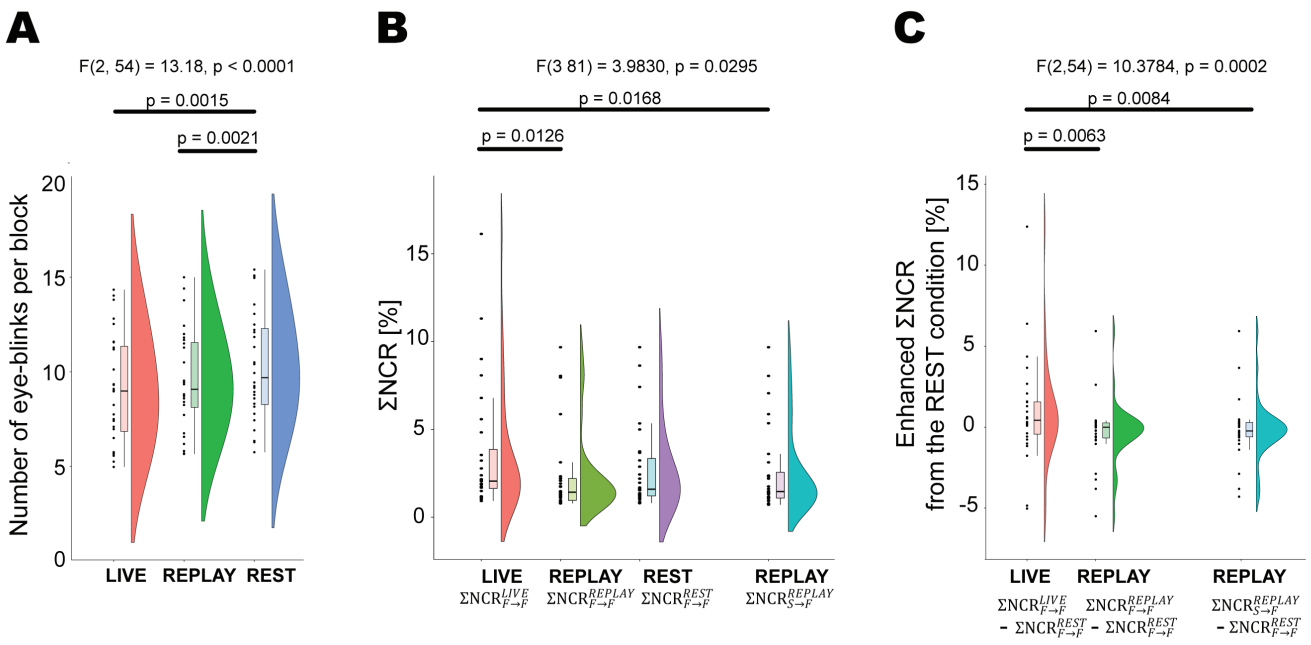

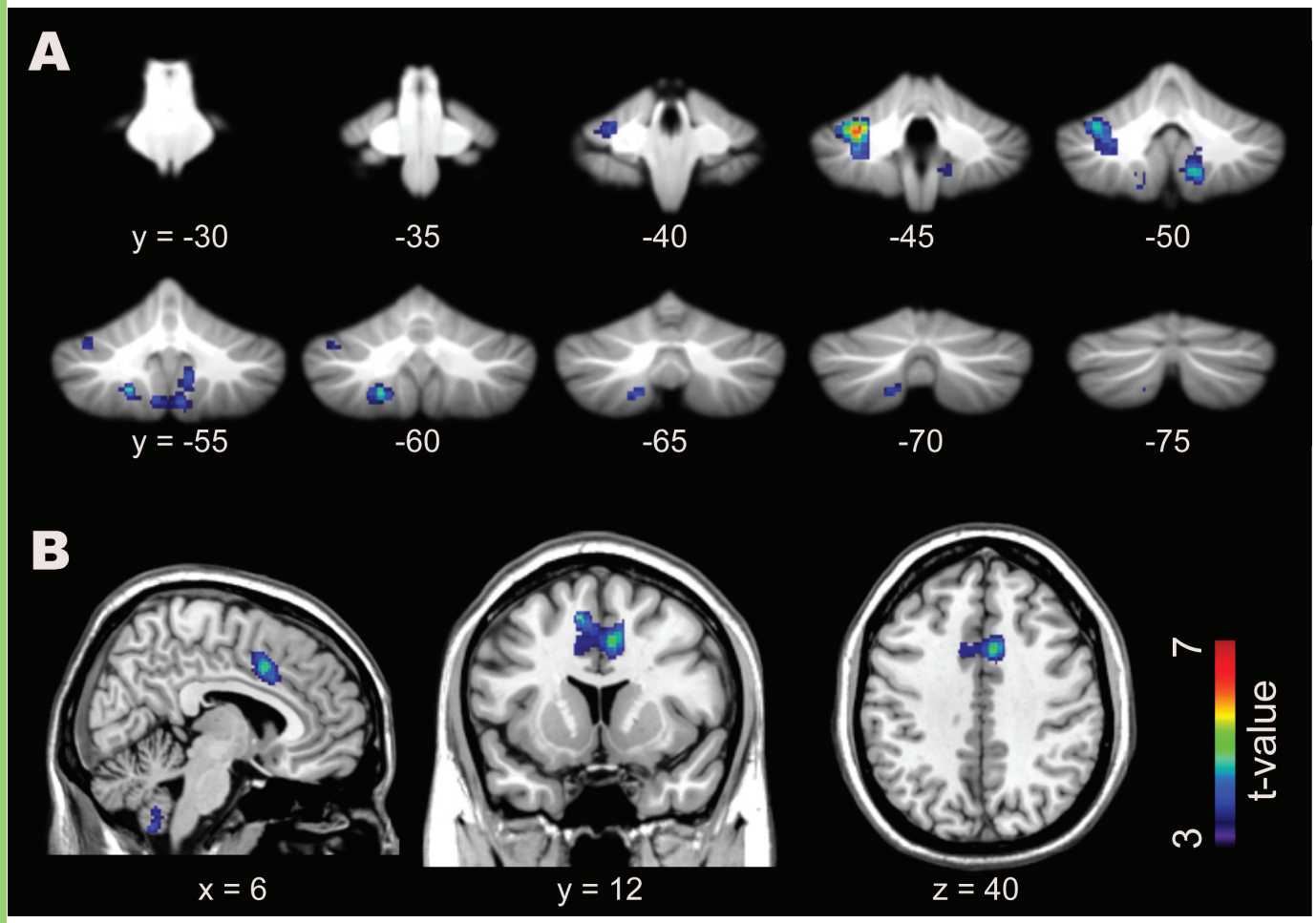

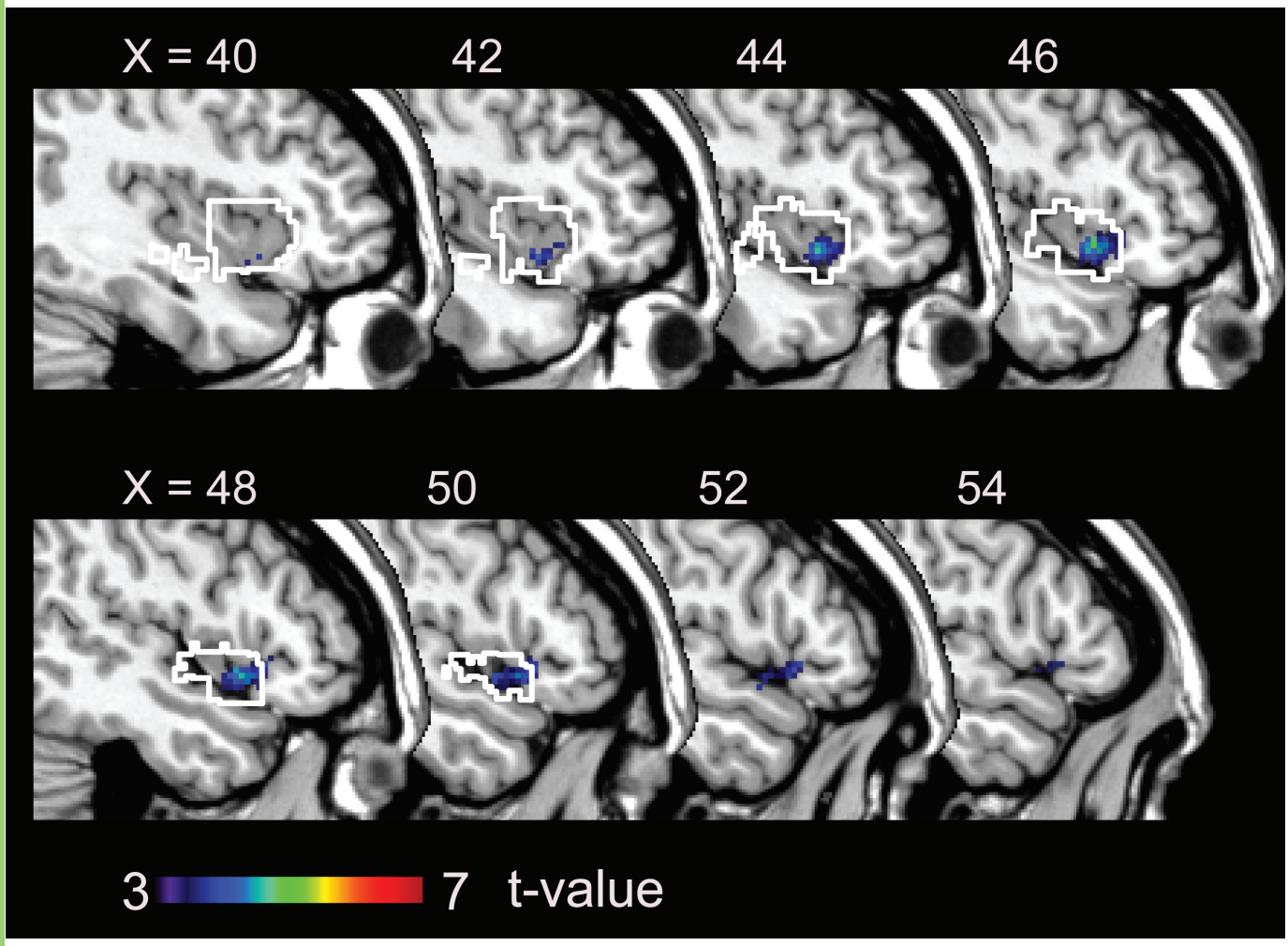

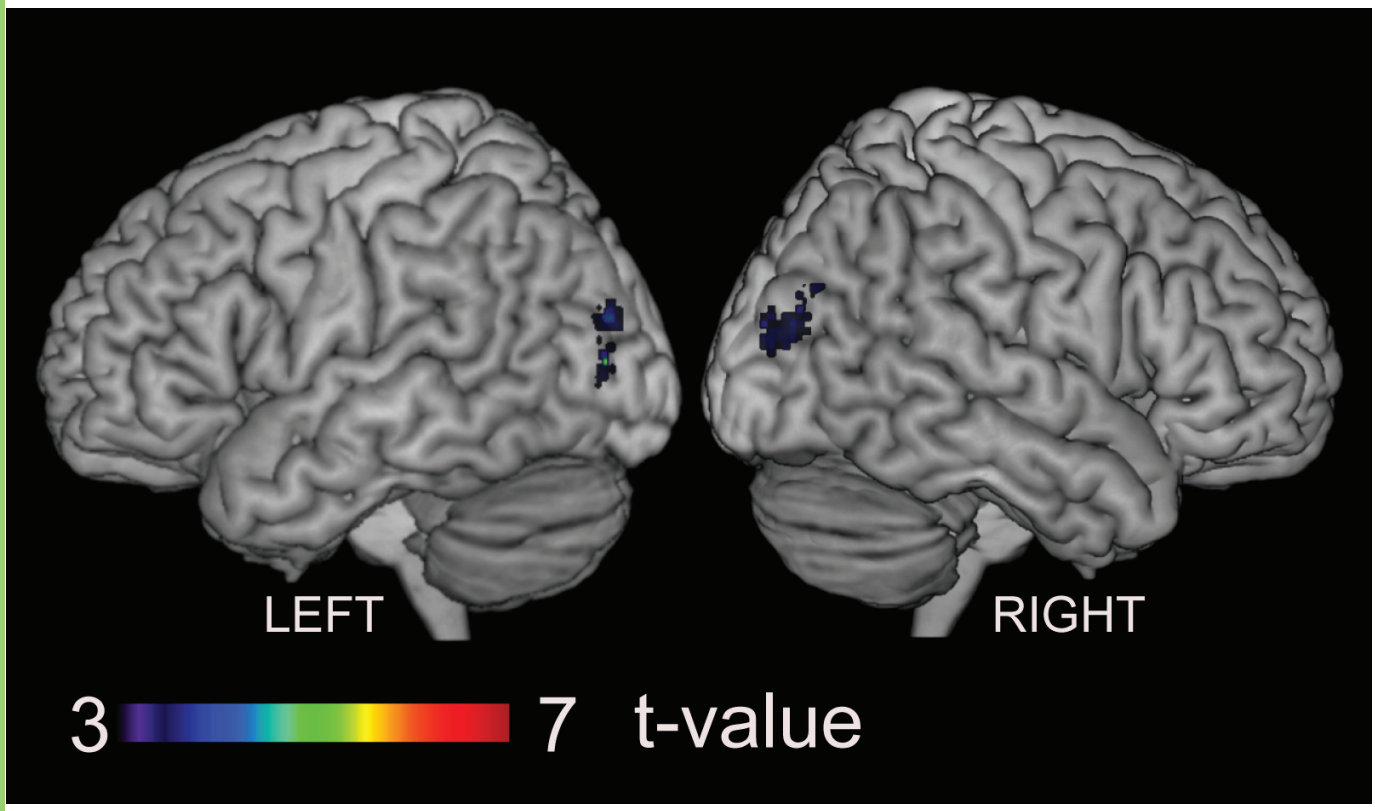

Tables 1

Location		Data Type	Data structure	Type of test	Multiple comparison correction	Program	Statistics	p-values	Power / Confidence interval
Manuscript	Figure								
a	3A	Number of eye blinks	Normal distribution	One-way repeated ANOVA	--	R	F(2,54) =13.1814	**p<0.0001**	η_g^2 = 0.03540
b		Number of eye blinks	Normal distribution	t-test (Post-hoc test, LIVE vs REST)	Bonferroni	R	T(27)=3.9464	**p=0.0015**	mean = -1.2757 (-1.9389 to -0.6124)
c		Number of eye blinks	Normal distribution	t-test (Post-hoc test, REPLAY vs REST)	Bonferroni	R	T(27)=3.8499	**p=0.0021**	mean = -0.7946 (-1.2182 to -0.3711)
d		Number of eye blinks	Normal distribution	t-test (Post-hoc test, LIVE vs REPLAY)	Bonferroni	R	T(27) = 2.3522,	p=0.0786	mean = -0.4810 (-0.9006 to -0.0614)
e	3B	Absolute ΣNCR	Normal distribution	One-way repeated ANOVA	--	R	F(3,81)=3.9830	**p=0.0295**	η_g^2 = 0.03236
f		Absolute ΣNCR	Normal distribution	Paired t-test (Post-hoc test,	Bonferroni	R	T(27)=3.406	**p = 0.0126**	mean = 1.2294

				LIVEFF vs REPLAYFF)					(0.4888 to 1.9700)
g		Absolute ΣNCR	Normal distribution	Paired t-test (Post-hoc test, LIVEFF vs RESTFF)	Bonferroni	R	T(27)=1.4598	p = 0.9354	mean = 0.8888 (-0.3604 to 2.1379)
h		Absolute ΣNCR	Normal distribution	Paired t-test (Post-hoc test, LIVEFF vs REPLAYSF)	Bonferroni	R	T(27)=3.2934	**p = 0.0168**	mean = 1.0455 (0.3941 to 1.6969)
i		Absolute ΣNCR	Normal distribution	Paired t-test (Post-hoc test, REPLAYFF vs RESTFF	Bonferroni	R	T(27)=0.9065	p = 1.0000	mean = -0.3406 (-1.1116 to 0.4304)
j		Absolute ΣNCR	Normal distribution	Paired t-test (Post-hoc test, REPLAYFF vs REPLAYSF	Bonferroni	R	T(27)=1.2083	p = 1.0000	mean = -0.1838 (-0.4960 to 0.1284)
k		Absolute ΣNCR	Normal distribution	Paired t-test (Post-hoc test, RESTFF vs REPLAYSF	Bonferroni	R	T(27)=0.4349	p = 1.0000	mean = 0.1568 (-0.5829 to 0.8965)
l		Absolute ΣNCR	Normal distribution	One-way repeated ANOVA	--	R	F(3,69)=4.3334	**p=0.0074**	η_g^2= 0.0785

m		Absolute ΣNCR	Normal distribution	Paired t-test (Post-hoc test, LIVEFF vs REPLAYFF)	Bonferroni	R	T(23)=3.0965	**p=0.0306**	mean = 1.0291 (0.3416 to 1.7165)
n		Absolute ΣNCR	Normal distribution	Paired t-test (Post-hoc test, LIVEFF vs RESTFF)	Bonferroni	R	T(23)=1.0783	p=1.0000	mean = 0.4588 (-0.4214 to 1.3390)
o		Absolute ΣNCR	Normal distribution	Paired t-test (Post-hoc test, LIVEFF vs REPLAYSF)	Bonferroni	R	T(23)=3.0779	**p=0.0318**	mean = 0.7771 (0.2548 to 1.2994)
p		Absolute ΣNCR	Normal distribution	Paired t-test (Post-hoc test, REPLAYFF vs RESTFF	Bonferroni	R	T(23)=1.9902	p=1.0000	mean = -0.5702 (-1.1630 to 0.0225)
q		Absolute ΣNCR	Normal distribution	Paired t-test (Post-hoc test, REPLAYFF vs REPLAYSF	Bonferroni	R	T(23)=1.4744	p=0.9234	mean = -0.2519 (-0.6054 to 0.1015)
r		Absolute ΣNCR	Normal distribution	Paired t-test (Post-hoc test, REPLAYFF vs REPLAYSF	Bonferroni	R	T(23)=1.1336	p=1.0000	mean = 0.3183 (-0.2626 to 0.8992)

s	3C	Relative ΣNCR	Normal distribution	One-way repeated ANOVA	--	R	F(2,54)=10.3784	**p = 0.0002**	η_g^2= 0.0483
t		Relative ΣNCR	Normal distribution	Paired t-test (Post-hoc test, LIVEFF vs REPLAYFF	Bonferroni	R	T(27)=3.4061	**p = 0.0063**	mean = 1.2294 (0.4888 to 1.9700)
u		Relative ΣNCR	Normal distribution	Paired t-test (Post-hoc test, LIVEFF vs REPLAYSF	Bonferroni	R	T(27)=3.2934	**p = 0.0084**	mean = 1.0455 (0.3941 to 1.6969)
v		Relative ΣNCR	Normal distribution	Paired t-test (Post-hoc test, REPLAYFF vs RESTSF	Bonferroni	R	T(27)=1.2083	p = 0.7122	mean = -0.1838 (-0.4960 to 0.1284)
w		Relative ΣNCR	Normal distribution	One-way repeated ANOVA	--	R	F(2,40)=7.9233	**p=0.0013**	η_g^2= 0.1330
x		Relative ΣNCR	Normal distribution	Paired t-test (Post-hoc test, LIVEFF vs REPLAYFF	Bonferroni	R	T(20)=2.8343	**p=0.0306**	mean = 7805 (0.0102 to 0.0250)
y		Relative ΣNCR	Normal distribution	Paired t-test (Post-hoc test, LIVEFF vs REPLAYSF	Bonferroni	R	T(20)=2.9034	**p=0.0264**	mean = 0.8362 (0.0088 to 0.0167)
z		Relative ΣNCR	Normal distribution	Paired t-test (Post-hoc test,	Bonferroni	R	T(20)=0.6790	p=1.0000	mean = 0.0558

				REPLAYFF vs RESTSF					(-0.1156 to 0.2271)
aa	--	Absolute ΣNCR	Normal distribution	Repeated ANOVA, Main effect of conditions	--	R	F(3, 81)=3.9830	**p=0.0106**	η_g^2= 0.0132
bb		Absolute ΣNCR	Normal distribution	Repeated ANOVA, Main effect of sessions	--	R	F(3,81)=1.0351	P=0.3816	η_g^2= 0.0139
cc		Absolute ΣNCR	Normal distribution	Repeated ANOVA, Interaction (session x condition)	--	R	F(9, 243)=1.8235	p=0.0647	η_g^2= 0.0128
dd	4	fMRI (BOLD activation)	Normal distribution	Paired t-test (LIVE > REPLAY)	Random effect model at cluster-level inference	SPM	--	--	--
ee		fMRI (BOLD activation)	No assumption	Paired t-test (LIVE > REPLAY)	Nonparametric permutation test at cluster-level inference	SnPM	--	--	--
ff	5	fMRI (PPI value)	Normal distribution	Paired t-test (LIVE > REPLAY)	Random effect model at cluster-level inference	SPM	--	--	--

gg		fMRI (PPI value)	No assumption	Paired t-test (LIVE > REPLAY)	Nonparametric permutation test at cluster-level inference	SnPM	--	--	--
hh	6	fMRI (Normalized inter-brain sync)	Normal distribution	Paired t-test (LIVE > REPLAY)	Random effect model at cluster-level inference	SPM	--	--	--
ii		fMRI (Normalized inter-brain sync)	No assumption	Paired t-test (LIVE > REPLAY)	Nonparametric permutation test at cluster-level inference	SnPM	--	--	--

Table 2

Cluster level inference			Peak level inference		T-value	MNI coordinates			Side	Location	Probability
P_{FWE}		Cluster size mm^3	P_{FWE}								
SPM	SnPM		SPM	SnPM		X	Y	Z			
0.015	**0.025**	2616	0.960	0.443	3.848	-40	-60	-30	L	Cerebellum	Lobule VIIa crus I (Hem) (99%)
			0.006	0.001	6.734	-28	-46	-30	L	Cerebellum	Lobule VI (Hem) (85%)
			0.642	0.195	4.406	-28	-44	-44	L	Cerebellum	
0.010	**0.022**	2880	0.408	0.111	4.720	-18	-60	-52	L	Cerebellum	Lobule VIIIb (Hem) (68%)
			0.846	--	4.119	-6	-54	-54	L	Cerebellum	Lobule IX (Hem) (80%)
			0.954	--	3.870	-14	-52	-52	L	Cerebellum	Lobule IX (Hem) (67%)
			0.815	0.283	4.169	6	-56	-56	R	Cerebellum	Lobule IX (Hem) (86%)
			0.495	0.139	4.598	12	-50	-50	R	Cerebellum	Lobule IX (Hem) (87%)
0.002	**0.014**	4176	0.274	0.069	4.945	-8	10	50	L	Pre-SMA	
			0.986	0.532	3.702	-10	10	38	L	ACC	
			0.274	0.069	4.945	6	12	40	R	ACC	
0.056	**0.040**	1824	0.227	0.055	5.044	-8	-46	-22	L	Cerebellum	
			0.463	0.127	4.641	0	-56	-26	R	Cerebellum	Fastigii Nucleus (37%)
			0.471	0.130	4.630	14	-52	-30	R	Cerebellum	

ACC, Anterior cingulate cortex; Pre-SMA, Pre-supplementary motor area; MNI, Montreal Neurological Institute; Hem, Hemisphere

Table 3

Cluster level inference			Peak level inference		T-value	MNI coordinates			Side	Location	Probability
P_{FWE}		Cluster size mm^3	P_{FWE}								
SPM	SnPM		SPM	SnPM		X	Y	Z			
0.000	0.0824	1208	0.868	0.378	5.063	46	14	-6	R	Insular	
			1.000	1.000	3.545	54	14	-4	R	IFG	BA44 (21%)
			1.000	--	4.156	50	20	-4	R	IFGOr	BA45 (31%)

IFG, Inferior frontal gyrus; IFGOr, Inferior frontal gyrus (pars opercularis); Montreal Neurological Institute; BA, Brodmann area

Table 4

Cluster level inference			Peak level inference		T-value	MNI coordinates			Side	Location	Probability
P_{FWE}		Cluster size mm^3	P_{FWE}								
SPM	SnPM		SPM	SnPM		X	Y	Z			
0.001	0.2258	1088	0.999	0.829	5.753	-26	-82	4	L		
			1.000	0.999	4.695	-34	-78	4	L	MOG	
			1.000	0.999	4.628	-28	-86	22	L	MOG	
0.007	0.2852	880	1.000	0.998	4.739	28	-76	24	R	MOG	
			1.000	1.000	3.983	38	-80	16	R	MOG	
			1.000	1.000	3.827	34	-88	18	R	MOG	hOc4lp (35.4%)

MOG, Middle Occipital Gyrus; Montreal Neurological Institute